8-2004

The Effects of the Surface Nanocrystallization and Hardening (SNH) Process on Fatigue Resistance

Yuan Wei
University of Tennessee - Knoxville

To the Graduate Council:

I am submitting herewith a thesis written by Yuan Wei entitled "The Effects of the Surface Nanocrystallization and Hardening (SNH) Process on Fatigue Resistance." I have examined the final electronic copy of this thesis for form and content and recommend that it be accepted in partial fulfillment of the requirements for the degree of Master of Science, with a major in Materials Science and Engineering.

Peter K. Liaw, Major Professor

We have read this thesis and recommend its acceptance:

Raymond A. Buchanan, Hahn Choo

Accepted for the Council:
Dixie L. Thompson

Vice Provost and Dean of the Graduate School

(Original signatures are on file with official student records.)

To the Graduate Council:

I am submitting herewith a thesis written by Wei Yuan entitled “The Effects of the Surface Nanocrystallization and Hardening (SNH) Process on Fatigue Resistance”. I have examined the final electronic copy of this thesis for form and content and recommend that it be accepted in partial fulfillment of the requirements for the degree of Master of Science, with a major in Materials Science and Engineering.

Dr. Peter K. Liaw

Major Professor

We have read this thesis
and recommend its acceptance:

Dr. Raymond A. Buchanan

Dr. Hahn Choo

Accepted for the Council:

Dr. Anne Mayhew

Vice Chancellor and Dean of
Graduate Studies

(Original signatures are on file with official student records)

The Effects of the Surface Nanocrystallization and Hardening (SNH) Process on Fatigue Resistance

A Thesis
Presented for the
Master of Science Degree
The University of Tennessee

Wei Yuan
August 2004

Acknowledgement

I'm indebted to many people who have helped me during my master degree study. My advisor, Dr. Peter K. Liaw, has been kindly helping me with my research throughout these years, creating environments for me to extend my potentials, and providing all kinds of opportunities for me to develop my academic capabilities and interpersonal skills. Dr. Leon L. Shaw of the University of Connnecticut has been giving me precious instructions on my research, providing all the necessary materials for the project, and helping me greatly in my research work. Dr. Raymond A. Buchanan and Dr. Hahn Choo, who kindly agreed to be on my committee, have been giving all kinds of help to me, making it possible for me to finish my master degree study. They have been encouraging me on my research work and on every step of my progress.

Mr. Douglas E. Fielden at the University of Tennessee (UT) has always been a great friend and making every effort possible to help me get the work done in a timely manner. His expertise in the equipment design and machining techniques has been the accelerator in making progress in this project.

In the process of my study, many people helped me on many aspects that are indispensable. I'm thankful to Dr. John R. Dunlap, Mr. Jones Greg, and Ms. Xiaoyun Lin for helping me on the operation of Transmission-Electron Microscopy, Scanning-Electron Microscopy, and X-ray diffractometer. I am thankful to Dr. Joseph E. Spruiell for his kind instruction on the X-ray technique.

Many thanks to Mr. Chris Stephens, Mr. Kaixiang Tao, Dr. Hongbo Tian, Dr. Bing Yang, Mr. Juan Villegas, Mr. Yulin Lu, Mr. Gongyao Wang, Mr. Daifeng Wang,

Mr. Yan Cui, Mr. Robert McDanials, Mr. Jawan Tian, Ms. Sujing Xie, Ms. Dongchun Qiao, Ms. Lang Huang, Mr. Zenghu Han, and Mr. Fengxiao Liu for their kind help.

Acknowledgements are due to the financial support for this research by the National Science Foundation with the program on "The Novel Surface Nanocrystallization and Hardening (SNH) Process for Improved Fatigue and Wear Resistance" under Grant No. - DMR-0207729, and the Combined Research-Curriculum Development (CRCD) Program under EEC-9527527 and EEC-0203415.

Abstract

Nanocrystalline and coarse-grained materials have shown high resistances for the fatigue-crack initiation and growth, respectively. In this thesis, the surface-mechanical-attrition (SMA) treatment has been employed for the surface-nanocrystallization and hardening (SNH) process to produce engineered materials with coarse grains in the interior and grain-refinement progressively down to the nano-size on the surface.

The effects of the different processing parameters of the SMA treatment, including the ball size, materials, and treatment time, on the SNH process of the Ti-6Al-4V and Ni-based Hastelloy® C-2000 Alloys were investigated from the viewpoints of the microstructure, microhardness, surface roughness, and fatigue behavior, by means of the optical microscopy, scanning-electron microscopy, transmission-electron microscopy, X-ray diffraction, Vickers-microhardness indentation, three-dimensional (3D) non-contact scanning white light interferometry profilometer, as well as four-point-bend tests.

The surface-grain refinement was found in all the samples. The surface hardness was improved in the Ni-based Hastelloy® C-2000 superalloys. After the treatment, the surface roughness definitely increased. The fatigue results and fractographes showed that the SMA treatment could improve the fatigue lives. However, the longer-time plus greater-size-balls treatment has the adverse effect on the fatigue lives. The fatigue behaviors of the treated samples were highly influenced by the adhesion-fracture region

on the surfaces due to the interaction between the balls and the sample surface during the treatment.

Further research activities were suggested in this thesis.

Table of Contents

List of Tables

List of Figures

1. Introduction

The surface of the engineering materials plays an important role in affecting their durability during service. The surface will directly contact the environment and undergo the corrosion, wear, etc. It is well known that the surfaces of structures are the most susceptible regions to fatigue failures, and fatigue cracks are generally initiated at the surfaces. Since failures due to repeated loading accounts for at least half of all mechanical failures, the fatigue performance of materials has the prime importance for the design of structures, which are subjected to cyclic loading [1]. Hence, strengthening of the material at or very close to the surfaces is quite important in enhancing fatigue lives.

The strengthening strategy can be achieved by various mechanical and/or thermo-chemical surface treatments. Besides strengthening the surface layers, the creation of residual compressive stresses at the surface is also important. Both approaches can be realized by the application of suitable surface-treatment methods, such as laser processing [2-6], coating, caburization [7-14], nitridation [15], nitricaburization [16-18], shot peening [19-22], deep rolling, etc. Those methods effectively enhance the surface-mechanical properties of metals, and, thus, improve the performance of the engineering materials in service.

Nanocrystalline materials, which are structurally characterized by nanometer-sized grains with a large number of grain boundaries, have been found to exhibit many unique properties, relative to their coarse-grained counterparts. For example, most nano-metals and alloys possess high strengths and hardnesses [23-25]. With increasing

the evidences of novel properties in nano-materials, it is reasonable to achieve the surface modification by the generation of a nanostructured surface layer so that the overall properties and behavior of the material are significantly improved. This kind of surface modification has been referred as surface nanocrystallization (SNC).

Nanostructured-surface layers can be produced by means of various coating and deposition techniques, such as the physical-vapor deposition (PVD), chemical-vapor deposition (CVD), and plasma processing. However, the surface-mechanical-attrition (SMA) technique has shown the advantages, compared with the coating and deposition methods for the SNC. For example, there is no change in chemical compositions of the nanostructured surface and in the interior, as well as a gradient variation in the grain dimension from the nano-size grains in the top layer to coarse grains in the interior. However, the bonding of the nanostructured surface layer with the matrix will not be a problem in the surface-mechanical-attrition technique.

From the objectives of improving the fatigue resistance, nano-grains on the surface will increase the surface strength, which will translate into the suppression of fatigue-crack initiation, and the coarse grains in the interior of the component will provide the resistance to fatigue-crack growth at the low stress intensities. Such an engineered microstructure gives the best combination of the resistances to fatigue-crack initiation and growth.

In this project, we will study the fatigue behavior of different materials treated by the SMA technique. At the same time, the microstructure, microhardness profile,

surface roughness, fatigue-fracture surface, surface-elemental distribution will be investigated.

2. **L**iterature **R**eview

In this section, the shot peening and surface-mechanical attrition (SMA) are reviewed for their effects on the materials-surface properties. Although these two techniques are involved in using high-energy balls to impact the material surfaces and introduce the plastic deformation, there are many differences between them. In the shot peening, the shots are micrometer-sized balls, including the steel particles, powders, even the gas, which have the high speed and flux. The interaction between the shot and the surface occurs only one time. In the SMA, the size of the balls is 5-10 millimeters in the diameter, and the number of the balls is limited. The processing is performed in a chamber that has a controlled atmosphere. The interaction between the balls and the sample surface can occur many times. The key difference between them is the greater sized ball used in the SMA than in the shot peening. These larger balls in the SMA have higher energies and can introduce more localized plastic deformation to result in the grain refinement progressively down to a nanometer region in the surface layer. We also reviewed the fatigue behavior of the nano- and ultrafine-grained materials.

2.1 Shot Peening

The shot peening is a process in which superficial compressive residual stresses are introduced to a component by means of the bombardment with shots, such as spherical steel particles, powders, or gases. Shot peening is an effective method of improving the fatigue strength of components. A series of effects can be introduced by

the shot peening. These effects include the formation of nano-grains and the compressive stresses on the surface layer.

2.1.1 Nanostructured Surface Layer

Tao et al. [19] used the ultrasonic shot-peening method to introduce the nanocrystalline on the surface of iron. By transmission-electron microscopy (TEM), they found that the grain sizes on the sample surface, treated 450 seconds and 250 seconds, reached 10 nm and 16 nm, respectively.

2.1.2 Residual Stresses

The surface treated by the shot peening will have the compressive residual stress on the surface. Menig et al. studied the residual-stress profiles of the AISI 4140 steel by the shot peening with an air-blast machine [20]. It was observed nondestructively by neutrons and X-rays. The surface layer of the AISI 4140 steel is under the compressive stress, and the underneath layer is subjected to the tensile stress.

2.1.3 Fatigue Resistance

The shot peening not only introduces the surface-strengthened layer, but a compressive residual stress at and near the exposed surface layers of the components by the surface-plastic deformation. This trend retards or eliminates the initiation and propagation of fatigue cracks and, consequently, plays an important role in the improvements of fatigue limits.

Song et al. [21] did the research regarding the effect of shot peening on the crack-closure and crack-growth behavior. After shot peening, the steady-state crack-growth region was interrupted, and crack retardation began. A period of cycles was taken for the exhaustion of the shot-peening effect. The crack propagated at a baseline of 7.8×10^{-5} mm/cycle before peening. Subsequently, this propagation rate was retarded and fell to a minimum value approaching 5.7×10^{-6} mm/cycle at a crack length of 15.50 mm.

Drechsler et al. [22] showed the relationship of the fatigue life of the Ti-10V-2Fe-3Al alloy with the shot-peening intensity at $\sigma_a * k_t$ = 1,100 MPa ($\sigma_a * k_t$ is the maximum notch-root stress, k_t is the notch-stress-concentration factor, and σ_a is the applied stress amplitude). First the fatigue life increases with the peening intensity[1], and, then, slightly decreases after the shot peening with very high intensities. The fatigue life was increased by the shot peening, and there is an optimal intensity for the treatment. This trend can be explained as follows. The shot peening, in one hand, increases the surface compressive stress of the components that improves the fatigue resistance. On the other hand, it also increases the roughness of the surface, increases the stress concentration of the surface, and induces more crack-initiation sites, which, thus, reduces the fatigue life.

2.2 Surface-Nanocrystallization and Hardening (SNH) by the SMA

The SMA is proposed, based on two established phenomena. The first phenomenon is the mechanical alloying, by which nano-powders can be produced by

repeatedly impacting micrometer-sized powders with high-energy balls [24, 25]. The second phenomenon is the introduction of compressive residual stresses at the surface layer through shot peening [16].

The SMA is an effective approach to create the localized plastic deformation, resulting in the grain refinement progressively down to the nanometer region in the surface layer of metallic materials [19, 26]. This technique has been successfully applied in achieving SNC in a variety of materials, including pure metals, alloys, and steels [23, 25, 26].

The surface nanocrystallization has a great potential in industrial applications. For the further development of this technology, a clear understanding of the underlying mechanism for the formation of nanostructures during the treatment is necessary.

2.2.1 Microstructure

Lu's group [23, 25, 26] systematically investigated the microstructural evolution of the pure Fe and AISI 304 stainless steel by means of the SMA treatment. As the straining decreases from the maximum at the top-surface layer to zero in the matrix of the pure Fe, the microstructure characteristics at different depths from the deep matrix to the top surface are shown below [23].

Dislocations, dense dislocation walls and dislocation tangles

Three typical deformation-induced microstructure features were identified in the deformation layer at low strains adjacent to the strain-free matrix (60-80 μm deep from the top surface): a) dislocation lines (DLs), b) dense dislocation walls (DDWs), these

DDWs are parallel to each other separated with a uniform spacing, and the misorientations across DDWs are usually smaller than 1^o, and c) dislocation tangles (DTs) in some grains, the dislocation distribution is not uniform and arranged without preferable sliding orientations.

Grain subdivisions and subgrains.

As the depth decreases, deformation strains and strain rates increase. Most original grains are found to be subdivided into micro-sized cells, of which the shapes are either roughly equiaxed or lamellar in the cross section. The misorientations across the refined cell are found to be less than 1^o.

Nanostructures

The deformation strain and strain rate are drastically increased in the top-surface layer. Nano-sized microstructures were observed in the regime from 15 μm in depth to the top surface. Close to the top surface, nano-sized equiaxed nanocrystallites are observed. The selected-area-electron-diffraction (SAED) pattern indicates small misorientations among these nano-grains. The misorientations between the neighboring nano-grains gradually increase to large angles with further straining. Then, equiaxed nano-grains with random orientations can be achieved.

2.2.2 Surface-Nanocrystallization Mechanism

Based on the microstructural features observed in various sections with different strains in the deformed surface layer, the following elemental steps are involved in the grain-refinement process:

1. the development of DDWs and DTs in the original grains and in the refined cells.

2. the transformation of DDWs and DTs into subboundaries with small misorientations separating individual cells or subgrains;

3. the evolution of subboundaries to highly misoriented grain boundaries.

2.3 Fatigue Properties of the Nano- and Ultrafine-Grained Alloy

The tension-tension fatigue behavior of the fine-grained 5058 Al alloy processed by the equal-channel-angular pressing (ECAP) is explored by Vinogradov et al. [27], who found that the ECAP treatment shows no improvement of the fatigue life in the low-stress region. However, in the high-stress region, at relatively high loads, the ECAP alloy endures a slightly higher number of cycles to failure than its conventional counterpart. The reason for this trend is that the grain refinement results usually in greater crack-initiation resistance and faster crack propagation. At the high stress level, the higher yield stress in the ECAP alloy prevents the macroscopic plastic deformation at the beginning of load-controlled cycling in contrast to the low-strength initial alloy. This, in turn, increases the incubation period for crack nucleation, and increases the total fatigue life in the fine-grained alloy. At the low stress level, two factors, (1) the low resistance to crack propagation, and (2) progressive softening during fatigue, will affect the high-cycle fatigue behavior of the ECAP alloy.

The fatigue-fracture surface in the ECAP specimens seems more brittle with a finer dimple pattern and visible crack-arrest markings. In the ECAP specimen, the crack propagates straight with very small deflections, while in the as-received material,

the crack grows in a zig-zag manner. These deflections are most likely induced by grain boundaries. In the larger grain, the crack deflection decreases the driving force for the crack advancement and retards cracking in materials. Thus, the larger-grained alloy has higher resistances to crack propagation than the ECAP-treated alloy at the low-stress-intensity region.

Hanlon et al. studied the grain-size effects on the fatigue response of the electrodeposited nanocrystalline pure Ni and a cryomilled ultrafine-crystalline Al-Mg alloy [28]. It was found that the grain refinement generally leads to an increase in the resistance to failures under stress-controlled fatigue, whereas a generally deleterious effect was seen on the resistance to the fatigue-crack growth.

3. **E**xperimental **P**rocedures

In order to investigate the effect of the SNH process realized by the SMA treatment on the fatigue resistance, two kinds of alloys have been employed in this research. They were the Ti-6Al-4V alloy and the Ni-based Hastelloy® C-2000 alloy. The four-point-bend-test method was used to study the fatigue resistance of the as-received and treated samples. The scanning-electron microscopy (SEM), transmission-electron microscopy (TEM), and X-ray diffraction (XRD) provided the microstructure information. The three-dimensional (3D) non-contact scanning white-light-interferometry profilometer was used to obtain the surface roughness of the treated sample with different treatment parameters. The fatigue facture surfaces were investigated by the SEM and energy-dispersive X-ray spectroscopy (EDS). The microhardness profiles along the cross-sectional surface were measured by the Vickers-hardness indentation.

3.1 Specimen Preparation

3.1.1 The Materials for the SMA Treatment

The Ti-6Al-4V alloy and the Ni-based Hastelloy® C-2000 alloy have been used for the SNH process. The titanium alloys have been widely used in the chemical and aerospace industries, and there have been considerable research efforts, using shot peening and nitriding to improve fatigue and wear resistances of Ti alloys, and the Ni-based Hastelloy® C-2000 superalloy also has been widely used in the chemical industries for its superior fatigue and corrosion resistance. The data generated from the

present research efforts will provide an excellent baseline for studying the efficacy of the SNH process.

The chemical compositions of the Ti-6Al-4V and Ni-based Hastelloy® C-2000 alloys are shown in Tables 1* and 2, respectively. The mechanical properties of the Ti-6Al-4V and Ni-based Hastelloy® C-2000 alloys are shown in Table 3.

The Ti-6Al-4V alloy is an alpha-beta alloy. The alpha-phase proportion usually varies from 60 to 90%. The typical microstructure is equiaxed or elongated alpha grains within a transformed beta matrix. The Ni-based Hastelloy® C-2000 superalloy is a single face-centered-cubic (FCC) structure.

3.1.2 Parameters of the Surface-Mechanical-Attrition (SMA) Process

Figure 1* shows a schematic of the machine for the SMA process to result in the surface nanocrystallization. As shown in Figure 1, the up-and-down oscillation of the process chamber is driven by an electric motor. The up-and-down oscillation of the chamber will force the balls inside the chamber to accelerate and impact the surfaces of the metallic plates locked at the top and bottom of the chamber. Adjusting the location of the connecting rod will change the impact velocity of balls.

Actually, our current samples treated by the SMA are processed in the Spex 8,000 mill (Figure 2). The balls used are steel or WC balls whose diameters are 9.7 mm, or 7.9 mm and 4.88 mm. The processing times are from 30 min. to 180 min., and all the

* All tables are located in Appendix A
* All figures are located in Appendix B

samples are processed in the argon (Ar) atmosphere at room temperature. These parameters used by SMA for the SNC are listed in the Table 4.

For the Ti-6Al-4V and Ni-based Hastelloy® C-2000 alloys, before the treatment, the discs were cleaned with acetone, then with ethanol. No other surface-conditioning treatment, such as polishing, coating, etc. was done. They were all treated in the Spex 8,000 mill at room temperature with Ar as the protection atmosphere.

The Ti-6Al-4V discs were bombarded by five stainless steel 440C balls in a diameter of 9.7 mm in the Ar atmosphere for 180 min. The composition of the 440C stainless steel balls was listed in the Table 5.

Ni-based Hastelloy® C-2000 alloy discs were bombarded by five WC/Co balls (94% WC and 6% Co in weight percent) with different times and ball sizes. The sizes of the balls were 4.88 mm and 7.9 mm in diameter, respectively. The processing times were 30 min., 60 min., and 180 min., respectively. The parameters of processing the Ni-based Hastelloy® C-2000 alloy are shown in Table 6.

The discs of the Ti-6Al-4V and Ni-based Hastelloy® C-2000 alloys were cut from the plates. The dimensions of the discs of Ti-6Al-4V and Ni-based Hastelloy® C-2000 alloys for the SMA treatment are listed in the Table 7. The diameter of the whole disc is 49 mm, and the diameter of the treated area by the SMA is 30 mm. The thickness of the Ti-6Al-4V disc is 5 mm, while that of the Ni-based Hastelloy® C-2000 disc is 3.22 mm.

The effects of different processing parameters used by the SMA method on the SNC are studied. Moreover, the results of the fatigue resistance, microstructure,

microhardness, and surface roughness are related to these processing parameters in order to optimize the SMA process.

3.2 Mechanical Testing and Microstructural Characterization

3.2.1 Fatigue Tests

The four-point-bend-test method has been used, because there is a constant bending moment inside the two inner pins, and the fatigue crack will initiate on the sample surface inside the two inner pins. It is suitable for testing the surface-crack-initiation resistance. The geometry of the fixture is shown in Figure 3. The distances of the inner pins and outer pins are 10 mm and 20 mm, respectively.

According to the American Society for Testing and Materials (ASTM) C 1211-92 *Standard Test Method for Flexural Strength of Advanced Ceramic at Elevated Temperature* [29], the fatigue specimens were cut from the treated discs of the Ti-6Al-4V and Hastelloy® C-2000 alloys by the electrical-discharge machining (EDM). The dimensions of the Ti-6Al-4V and Hastelloy® C-2000 fatigue samples are 25 mm × 2.5 mm × 2.0 mm and 25 mm × 3.22 mm × 3.22 mm, respectively, as shown in Table 8.

The tests have been conducted on a MTS 810 electrohydraulic machine at room temperature. The ratio R (= $\sigma_{min.}/\sigma_{max.}$, where $\sigma_{min.}$ and $\sigma_{max.}$ are the minimum and maximum applied stresses, respectively) is 0.1, and the frequency is 10 Hz.

The fatigue tests were performed under the load control. In order to obtain the stress versus fatigue-life curve, Equation (1) was used to convert the load into the stress.

$$\sigma = 3pl / 4bd^2 \tag{1}$$

where σ is the maximum stress on the surface, l is the distance of the outer pins, b is the width of the sample, d is the depth of the sample, and p is the maximum load.

3.2.2 Microstructure

Samples treated by SMA will possess the nano-layer on the surface, and the interiors of the sample have progressively to approach coarser grains. Optical microscopy (OM), SEM, TEM, and XRD were used to show the microstructures and grain sizes.

When observed by OM and SEM, the samples must be polished and etched. The Buehler Eomet Variable-Speed Grinder-Polisher was used for grinding and polishing. The samples were first ground using 120, 180, 240, 360, 400, 600, and 1,200 grit papers in succession. Between each step, the sample was rotated 90° to remove the previous scratches. Polishing was performed in two consecutive steps, first using a 6 μm diamond paste on a nylon cloth and, then, a 0.05 μm alumina paste on a micro-cloth.

About the etching, for the Ti-6Al-4V alloy, the etch reagent used is the Kroll's reagent (2 mL HF, 3 mL of HNO_3, and 100 mL of H_2O). The polished surface was swabbed for 20 seconds [30]. For the Hastelloy® C-2000 alloy, the electrochemical etching was used by immersing the alloy in the reagent (95 mL HCl and 5g Oxalic Acid) and etching for 5-10 seconds at 6 volts.

The TEM samples of different depths from the specimen surface were obtained first by (1) mechanically polishing on one side or two sides until the sample reached a

20 μm thickness, and (2) finally thinning by two-side jet with a solution of the 5% perchloric acid and 95% ethnol (in volume percent) at 10 □.

The Philips X'Pert X-ray Diffractometer with Cu K_α radiation ($\lambda_{K\alpha 1}$ = 0.154056 nm, and $\lambda_{K\alpha 2}$ = 0.154439 nm) was used to determine the surface composition. The values of the Full Width at Half Maximum (FWHM) were obtained by the peaks of $\lambda_{K\alpha 1}$ = 0.154056 nm.

3.2.3 Microhardness

Samples treated by the SMA undergo the plastic deformation on the surface. There will be the strain hardening and grain refinement on the surface, which will result in a microhardness profile along the cross section. The Vickers-hardness-indentation experiment was utilized to measure the hardness profile from the surface to the interior. The applied load is 300 g.

The cross-sectional surfaces of the samples for the microhardness measurement were first ground using 120, 180, 240, 360, 400, 600, and 1,200 grit papers in succession. Polishing was performed in two consecutive steps, first using a 6 μm diamond paste on a nylon cloth and, then, a 0.05 μm alumina paste on a micro-cloth.

3.2.4 Surface Roughness

The high-cycle four-point-bend-fatigue test is sensitive to the surface defects. The large surface roughness will cause the stress concentration to initiate the cracks. The fatigue life will be shortened.

The three-dimensional (3D) non-contact scanning white-light-interferometry profilometer was employed to measure the surface roughness.

(The detailed information about the operation could be found at: http://www.microphotonics.com/fogaletech.html)

3.2.5 Surface-Elemental Analyses

The SNC is realized by the SMA technique. The surface of the sample will be repeatedly impacted by the steel or WC balls. Similar to the ball milling [31, 32], the cold welding and fracture process will occur between the surfaces of the balls and samples.

The EDS and XRD were used to analyze the surface elements to reveal the interactions between the balls and the sample surface.

3.2.6 Fatigue-Fracture-Surface Analyses

The fracture surface, subjected to the four-point-bend-fatigue test, consists of two areas – fatigue-crack initiation sites at or near the surface and fatigue-crack-propagation region from the surface to the interior.

SEM was employed to investigate the fracture surface. More attention was paid to the crack-initiation sites to find the crack-initiation mechanism.

4. **R**esults and **D**iscussion

4.1 Ti-6Al-4V Alloy

4.1.1 Microstructure

The cross-sectional microstructures of the as-received and treated samples by SEM are shown in Figures 4 and 5. In Figure 4, the cross-sectional microstructures of the as-received sample are the alpha-beta structures. The depressed part is the alpha phase, and the raised part is the beta phase under the etching condition described in 3.2.2. The alpha and beta phases are uniform through the cross section. The surface of the as-received sample is very flat.

In Figure 5**,** the cross section of the treated sample shows the two distinct microstructures. From the surface to the interior, there are a white layer and a gray substrate. In the gray substrate, two areas – the SMA-affected zone, and the SMA-unaffected zone - are notable. From this figure, it can be found that there are more premature cracks running through the white layer. The thickness of this layer is about 25 μm. The white layer covers the whole treated surface.

Very near to the interface of the white layer and the Ti-6Al-4V substrate, the alpha and beta phases in the SMA-affected zone are almost stretched and mixed together and not easily to differentiate. Going to the interior, the microstructure of the SNH-unaffected zone is similar to that of the as-received sample.

Using EDS (Figure 6), the white layer (Figure 6a) shows a very high concentration of Fe, while the alpha (Figure 6b) and beta phase (Figure 6c) exhibit the higher contents of the Ti. This white layer is the adhesion-fracture region. Its formation

is due to the interaction of the surfaces of the steel balls and sample. When the steel balls impacted the sample surface, the adhesion process occurred. After the balls bounced away from the sample surface, a separation process of the balls surface and the sample surface took place. With the treatment continued, the adhesion and separation process continued, and the more material of the steel balls was left on the sample surface, which results in a white layer.

4.1.2 Microhardness Profile

Vickers-microhardness measurements were taken across the thickness direction of the SMA-processed samples at the as-polished condition in 3.2.2. The result of the microhardness profile in Figure 7 showed that the SMA could not improve the surface microhardness. The variation of the microhardness along the cross section is relatively small with the maximum value being about 316 HV and the minimum value 284 HV. This kind of fluctuation may be due to the two-phase microstructure of the Ti-6Al-4V, and the microhardnesses of the alpha and beta phase are different.

4.1.3 Four-Point-Bend-Fatigue Result

The fatigue results are displayed in Figure 8. The fatigue lives of the SMA-treated samples are similar to those of the as-received samples at low stress levels ($\leq$600 MPa). At high-stress levels ($\geq$600 MPa), however, the SMA-treated samples appear to have slightly shorter lives than the as-received samples. This is most likely due to the presence of the surface cracks in the SMA-treated samples in Figure 5. Any

one of those surface cracks could provide a fatigue-crack-initiation site. Nevertheless, the short life at high-stress levels could also be due to the easy crack initiation on the surface of the SMA-treated samples, where the ductility is expected to be lower than that of the as-received surface.

4.1.4 Fractography

The fracture surfaces of the as-received (Figure 9) and the SMA-treated samples (Figure 10) show very different mechanisms of failures. The SMA-treated material presents a brittle ledge that is approximately 200 μm wide near the surface. The thickness of this ledge is similar to the depth of the SMA-affected zone. The SMA-treatment lowered the surface ductility.

The fracture surface of the as-received sample is flatter from the surface to the interior. This may be due to its homogeneous structure along the cross section.

4.2 Ni-based Hastelloy® C-2000 Superalloy

4.2.1 Microstructure

The cross-sectional microstructures of the as-received and treated samples by optical microscopy (OM) are shown in Figure 11. In Figure 11a, it can be seen that the grain size of the as-received sample is quite uniform from the surface to the interior, and the size is about 80 – 100 μm. The twins due to the rolling process were clearly seen in the as-received sample. Figure 11b presents the microstructures of the Lot 1 sample that are 30 min. treated with five WC balls in a diameter of 7.9 mm. Although the grains

shown on the surface were severely deformed and closely compressed, the micrometer-size grains still could be observed on the surface. Figure 11c shows the microstructures of the Lot 2 samples 180 min. treated with five WC balls in a diameter of 7.9 mm, there are two distinct zones along the cross section: the near-surface SMA-affected zone and the interior unaffected zone. However, the detailed microstructures near the surface cannot be clearly recognized by the OM and SEM. Figure 11d exhibits the cross-sectional microstructures of the Lot-3 samples that were treated 60 min., with 5 WC balls in a diameter of 4.88 mm. Except the dents of the balls on the surface, we could not find any difference of the microstructures, compared with the as-received samples in Figure 11a.

Figure 12 shows more detailed surface structures of the Lot 2 samples by means of the SEM and TEM. In the Figure 12a of the SEM image, the area near the surface layer is smoother than that of the deeper surface layer. Employed the TEM, in the smooth area very near the surface, the nano-grains are found (Figure 12b), whose average grain size is about 10 ~ 20 nm. When going from the surface to the interior **(**Figure 12c**),** there are a large amount of intersected plastically-deformed twins. Going deeper (Figure 12d), one-directional parallel plastically-deformed twins were found. The stacking fault energy of the Ni-based C-2000 superalloy is low, and, thus, the mechanical twins are favored in the high strain plastic deformation [25].

The changes of the full width at the half maximum (FWHM) for different X-ray peaks are presented in Figure 13. The peak-profile breadth of the XRD is related to the grain-size variation and the microstrain in the grains. However, the low-angle-peak

breadth mainly relates to the grain size, and the high-angle-peak breadth is primarily affected by the microstrain in the grains [33]. It is interesting to note in the Figure 13 that at low reflection angles (e.g. $2\theta = 43.5^{o}$), the sample treated with WC balls of 7.9 mm in diameter for 180 min. has the largest width (and thus, the smallest grain size). However, at the high reflection angles (e.g. $2\theta = 90.2^{o}$), the sample treated with WC balls of 7.9 mm in diameter for 30 min. exhibits the largest width, while the sample treated for 180 min. has the smallest width among the three kinds of treated samples. This result suggests that the sample treated for 180 min. has the lowest lattice microstrain. If the lattice microstrain is induced by dislocations, the sample treated for 180 min. has the lowest dislocation density. One possible explanation will be that the dense dislocations generated at the early stage of the SMA treatment rearrange themselves and become grain boundaries leading to the formation of nano-grains containing few dislocations. Therefore, there are more lattice microstrains in the samples treated for 30 min. and 60 min. than that in the sample treated for 180 min. However, the present explanation remains to be conformed by the detailed TEM investigation.

The results of the FWHM at low angle peaks are consistent with the change of grain sizes as a function of the processing conditions as presented in the Figures 11 and 12, in which, the surface of the 180 min. treated sample showed the nano-grains, and the micro-sized grains on the surface of the treated 30 min. sample and 60 min. samples were deformed.

Hence, the conclusions of this part are reached: 1) the surface of the treated 180 min. sample with 7.9 mm balls has nano-grains. The other two kinds of samples possibly have nano-grains on the surface, since their values of the FWHM at the low angle-peak are greater than that of the as-received sample. 2) The effect of the ball size for introducing plastic deformation is more significant than the time, because the grains on the surface of the treated 30 min. sample with 7.9 mm balls are more severely deformed than the treated 60 min. sample with 4.88 mm balls, as well as the FWHM values of the treated 30 min. sample with 7.9 mm balls are greater than the treated 60 min. sample with 4.88 mm balls, regardless of the X-ray results at the low angle or the high angle.

4.2.2 Surface Appearance and Elemental Analyses of the Fatigue-Tested Surface

Figure 14 shows the XRD profiles of the surfaces of as-received and SMA-treated samples. It can be found that there are no peaks of WC in the as-received sample, and in the SMA-treated sample surfaces, the peaks of WC appear. With increasing the treatment time and ball size, the intensity of the WC peaks increases. The height of the peaks of the WC goes up from the treated 60 min. sample with 4.88 mm balls to the treated 30 min. sample with 7.9 mm balls, and, then, to the treated 180 min. with 7.9 mm balls. This trend shows that the content of the WC on the surface of the treated 180 min. sample with 7.9 mm balls is the highest, and the content of the WC on the treated 60 min. sample with 4.88 mm balls is the lowest among the treated samples.

These results indicate that during the SMA treatment, the cold welding between the surface of the C-2000 superalloy and the WC balls occurred. When the balls bounced away from the surface of the sample, fracture occurred, and part of the materials of the ball was left on the surface of the sample. A greater ball and a longer time make this effect more pronounced.

The SEM images and EDS spectra of the surfaces of the as-received and as-treated samples are shown in Figure 15. It can be seen that the surface of the as-received sample is quite smooth and clean, while these of the treated samples are quite rough. The surfaces of the treated 30 min. and 60 min. samples have the scattered fragments of the fretting fracture. On the surface of the treated 180 min. sample, the treatment time is so long, and the amount of the fractured fragments produced by interactions between the surface of balls and the sample is so high, and fragments almost connect each other and cover the sample surface. It can also be noticed that the surface of the as-received sample does not contain the element of W, while the other three treated samples do. Furthermore, the treated 180 min. sample had the highest content of W with a percent of 15.91 atomic percent (at %), and the 30 min. treated with 7.9 mm balls sample and the 60 min. treated with 4.88 mm balls sample have W of 5.05 at % and 1.99 at % on the surface, respectively. The results of the EDS are consistent with the results of the XRD.

4.2.3 Surface Roughness

Figure 16 shows the surface roughness measured by the 3D non-contact profilometry. As shown in the colique plots of this figure, the surface of the as-received

sample is flatter than the surfaces of the treated samples. The histogram plot of the as-received sample is narrower than the treated samples. Among the treated samples, the histogram plot of the treated 180 min. sample is narrower than the other two kinds of treated samples. In the form of the peak-to-valley (PV), the root-mean-square average (rms) or the arithmetic-mean (Ra) values, the values of the treated samples are larger than the as-received sample. However, there is only a little difference in the treated sample. The treated 180 min. sample with 7.9 mm balls shows somewhat lower surface roughness than the treated 30 min. sample with 7.9 mm balls. The reason for this trend is that in the longer processing, the entire plate surface of the treated 180 min. sample has been impacted more times than the treated 30 min. sample, thus, the height of the peak regions is reduced, while the depth of the valleys will be not affected much by treated impacts. As a result, the PV value decreases slightly. With a longer treatment, the PV value does not change significantly because 1) the rate of generating peaks and valleys is in a dynamic equilibrium with the rate of reducing the height of peaks, and 2) the material has approached the strengthening saturation after repeated impacts [34].

4.2.4 Microhardness Profile along the Cross Section

In Figure 17, the SMA process improved the surface hardnesses of the treated 180 min. sample, and treated 30 min. sample with 7.9 mm balls and the treated 60 min. sample with 4.88 mm balls, i.e., from the value of 200 HV for the as-received sample to 430 HV, 400 HV, and 360 HV, respectively. We also noticed that the treated 180 min. treated sample and 30 min. sample with the same size of the balls have the similar

microhardness profiles. This may indicate that strengthening reaches the saturation point after the 30 min. of processing, even though the microstructure continues to evolve and the thickness of the nano-grain layer continues to grow after the 30-min. processing. The sample treated 60 min. with 4.88 mm balls has a shallower SMA-affected layer, whose thickness is approximately 220 μm, than the samples treated 30 min. and 180 min. with 7.9 mm balls, whose thickness is about 350 μm.

4.2.5 Four-Point-Bend-Fatigue Result

The applied stress vs. fatigue life (S-N) curves are presented in Figure 18. These results show that the treated 180 min. sample has a shorter fatigue life than the as-received sample regardless of the stress levels, while the other two SNH-processed samples have better fatigue resistances than the as-received sample, and the fatigue endurance limit has been improved greatly by the SMA treatment. The fatigue limits of the treated 30 min. sample and the treated 60 min. sample are improved to 600 MPa and 550 MPa, respectively, relative to the 400 MPa of the as-received sample, while the fatigue limit of the treated 180 min. sample is reduced to 350 MPa. These results indicate that the fatigue resistance can be improved by the SMA treatment, depending on the processing conditions. However, the processing condition should be optimized.

4.2.6 Fractography and Fatigue Resistance

The four-point-bend-fatigue life is affected by the properties of the sample surface, such as the roughness, microstructure, hardness, and residual stress. Figure 19

shows the fatigue-fracture surface of the as-received sample. In Figure 19b, it could be found that the crack-initiation site was below the surface, and the crack could initiate from grain boundaries. The crack steps in the grains around the crack-initiation site could be seen.

Figure 20 shows the fatigue-fracture surface of the treated 30 min. sample. In Figure 21a of the fracture surface of the treated 30 min. sample, the fatigue crack was found to initiate from a defect, which shows a different microstructure, relative to the material below. The EDS spectrum (Figure 21b) of the defect presents that this defect has the higher content of W, the same content as the surface of the treated 30 min. sample (Figure 15b). This defect is produced during the SMA process as discussed in the 4.1.1. Figure 22 shows the fatigue- fracture surface of the treated 180 min. sample. In Figure 23a, the fatigue crack of the treated 180 min. sample was noticed to initiate from the adhesion-fracture defect. By EDS (Figure 23b), this defect shows a very high content of W.

Although those two samples, treated 180 min. and 30 min. respectively, have the similar microhardness profiles, the similar surface roughness, and the similar fatigue-fracture surfaces, why do they have a large difference in the fatigue life? This trend can be attributed to the differences in the surface microstructure, and the residual stress. As discussed in the microstructure part, the treated 180 min. sample has a nano-layer on the surface. The long-time treatment may relax the surface-compressive stress (this trend needs to be verified by the measurement of the surface residual stress). As noticed in the Figures 15b and 15c, the fragments on the surface of the treated 30 min. sample

scattered, while on the surface of the treated 180 min. sample, the fragments induced by the interaction between the surface of the balls and sample almost connect each other and cover the surface. From the fatigue-fractured surface (Figures 21a and 23a), this trend can be discerned. The defect on the treated 180 min sample is thicker and denser than that on the treated 30 min. sample and the defects on the surface of the treated 30 min. sample are scattered. Since the surface of the treated 180 min. sample is covered by the WC layer, and the WC layer is very brittle, under the stress, the cracks easily initiate. However, the nano-layer in the 180 min. treated sample is below the WC layer, and it will not have the effect on resisting the fatigue crack initiation. At the same time, it has less fatigue crack growth resistance. So the fatigue crack very easily initiates and grows in the treated 180 min. sample. The scattering fretting defects on the treated 30 min. sample can only induce the stress concentration, and the fatigue crack still need more cycles to initiate, relative to the treated 180 min. sample.

In Figures 24 of the fatigue-fracture surface of the treated 60 min. sample with 4.88 mm balls, the crack-initiation site is below the surface. There are no defects near the crack-initiation sites. Since the treated 60 min. sample surface was hardened, the crack-initiation site showed brittle in Figure 24b, compared with the Figure 19b of the as-received sample. The greater hardness profile of the treated 60 min. sample than the as-received sample (Figure 17) also contribute to the greater fatigue endurance in the treated 60 min. sample (Figure 18).

In Figure 18, at the stress level less than 650 MPa, the fatigue resistance of the treated 30 min. samples with 7.9 mm balls is greater than that of the treated 60 min.

samples with 4.88 mm balls. This trend could result from the greater hardness profile in the treated 30 min. samples than the treated 60 min. samples (Figure 17). Similarly, greater fatigue resistances of the treated 30 min. and 60 min. samples than the as-received sample related to the greater hardness profiles in the treated samples (Figure 17). At this stress level range, the crack initiation is the dominance. The higher surface hardness, the longer time for the fatigue crack initiation. At the stress level of the 650 MPa, the fatigue resistances of the treated 30 min. and 60 min. samples and the as-received sample are similar. This trend may be due to crack-growth dominance at the high-stress level, namely, the fatigue life is primarily determined by the fatigue growth rate, not the fatigue-crack initiation. Because of this, those three kinds of samples may have the similar crack growth, thus, the similar fatigue resistance at the high stress level.

Summarizing the above results, the fatigue lives of the as-received and treated samples are affected by the microstructures, roughnesses, hardnesses, of the test samples.

5. Conclusions

Based on the above results and discussions, the following conclusions are reached:

(1) During the SMA process, the intense interactions between the surfaces of the balls and the treated sample will cause the cold welding and fretting fracture to occur during the SMA process. The longer treatment and the larger size balls used, the more obvious this interaction. The surface of the sample will be contaminated, and the adhesion-fracture fragments have different appearances on the surface. On the surface of the treated Ti-6Al-4V alloy using 9.7 mm stainless-steel balls, there is an adhesion-fracture layer with the premature cracks. For the Ni-based Hastelloy® C-2000 superalloy treated by the WC balls, on the surface of the 180 min. treated sample with 7.9 mm balls, there is a thin layer of the WC. The other two kinds of samples, 30 min. treated with 7.9 mm WC balls and 60 min. treated with the 4.88 mm balls, have the scattering adhesion-fracture fragments on the surface.

(2) In the Ti-6Al-4V alloy, the alpha and beta phases in the SMA-affected zone were stretched along the direction parallel to the surface, and mixed together. In the Ni-based hastelloy® C-2000 alloy, the surface micrometer-size grains of the as-received sample were refined by the SNH process to nanometers with the 180 min. treatment using 7.9 mm balls. Intersected plastically deformed twins and one-directional parallel twins were found at the deeper surface.

(3) In the Ti-6Al-4V alloy, the surface hardness was not improved by the SMA treatment. In the Ni-based Hastelloy® C-2000 alloy, the surface microhardness was

improved by the SMA treatment, relative to the as-received sample. The sample treated with 7.9 mm balls has a greater surface hardness and deeper hardened zone than the sample treated with 4.88 mm balls.

(4) The treated sample surfaces are rougher than the as-received samples in both the Ti-6Al-4V and the Ni-based Hastelloy® C-2000 alloys.

(5) The fatigue-life improvement is controlled by the surface roughness, microstructure, as well as hardness. In the Ti-6Al-4V alloy, the treated samples show the shorter fatigue life than the as-received sample at the high-stress levels. This is due to the premature cracks on the adhesion-fracture layer. In the Ni-based Hastelloy® C-2000 alloy, the 30 min. treated sample with 7.9 mm balls has best fatigue resistance. However, the 180 min. treated sample with the 7.9 mm balls has the worst fatigue resistance because of the brittle layer of WC on its surface.

6. Future Work

In order to have a complete understanding of the effects of the surface-nanocrystallization and hardening (SNH) process on the fatigue resistance, a more comprehensive study could be undertaken for this research. The surface-mechanical-attrition (SMA) treatment for the SNH still needs to be optimized by choosing the suitable balls sizes and processing time, which can result in a surface with a certain depth of a nano-grain layer and less surface defects. Although some work has been conducted on the microstructural characterization, it is still needed to reveal the microstructural evolution by TEM. Fully revealing the microstructures will open the door for us to deeply understand the mechanisms of SNC. More fatigue tests have to be performed, coupled with microstructural investigations. Other techniques, such as acoustic emission, and thermography, are needed to understand the mechanisms of the fatigue-crack initiation. The SMA treatment will induce the residual stress on the surface as the shot-peening process does. The residual-stress distribution needs to be measured by X-ray diffraction.

References Cited

1) H.O. Fuchs, R.I. Stephens. Metal Fatigue in Engineering. New York: John Wiley, 1980.

2) N.B. Dahaotre, A. Hunter, K. Mukherjee, Laser Surface Melting of W_2 Tool Steel: Effects of Prior Heat Treatment. J. Mater. Sci., 22 (1987) 403-406.

3) J.W. Elmer, M.A. Nweton, A.C. Smith, Transformation Hardening of Steel Using High-Energy Electron Beam. Weld J., 73 (1994) 291-299.

4) L.J. Yang, S. Jana, S.C. Tam, The Effects of Pre-Hardening on the Laser Transformation Hardening of Tool-Steel Specimens. J. Mater. Process. Technol., 25 (1991) 321-332.

5) C.R. Brooks, Principles of the Surface Treatment of Steels. Lancaster Technomic. Pub. Co., 1992.

6) E. Bourithis, A. Tazedakis, G. Papadimitriou, A Study on the Surface Treatment of "Calmax" Tool Steel by a Plasma Transferred Arc (PTA) Process. Journal of Materials Processing Technology, 128 (2002) 169-177.

7) T.B. Cameron, D.E. Diesburg, C. Kim, Fatigue and Overload Fracture of Carburized Steels. Journal of Metals, 35 (7) (1983) 37-41.

8) K. Genel, M. Demirkol, Effect of Case Depth on Fatigue Performance of AISI 8620 Carburized Steel. International Journal of Fatigue, 21 (1999) 207-212.

9) C.A. Apple, B. Krauss, Microcracking and Fatigue in Carburized Steel. Metallurgical Transactions, 4 (1973) 1195.

10) J.L. Pacheco, G. Krauss, Microstructure and High Bending Fatigue Strength in Carburized Steel. Journal of Heat Treatment, 7 (1989) 77.

11) S. Preston, Bending Fatigue Strength of Carburizing Steel SS2506. Materials Science Technology, 7 (1991) 105.

12) D.E. Diesburg, G.T. Eldis, Fracture Resistance of Various Carburized Steels. Metallurgical Transactions, 9A (1978) 1561.

13) G. Parrish, The Influence of Microstructure on the Properties of Case-Carburized Components. Heat Treatment of Metals, 4 (2) (1977) 45.

14) N. Krishnaraj, P.B. Srinivasan, K.J.L. Lyer, Optimization of Compound Layer Thickness for Wear Resistance of Nitrocarburized H11 Steels. Wear, 215 (1998) 123.

15) M. Guagliano, L. Vergani, Effect of Nitriding on Low-Cycle Fatigue Properties. Int. J. Fatigue, 19 (1997) 67-73.

16) G. Wahl, Component Properties After Salt Bath Nitrocarburizing by Tufftride Process. Heat treatment of Metals, 3 (1995) 65-73.

17) Y.H. Qiang, S.R. Ge, Q.J. Xue, Microstructure and Tribological Properties of Two-Step Nitrocarburized Steel. Wear, 218 (1998) 25.

18) P. Psyllaki, G. Kefalonikas, G. Pantaopoulos, S. Antoniou, J. Sideris, Microstructure and Tribological Behavior of Liquid Nitrocarburised Tool Steels. Surface and Coating Technology, 162 (2002) 67-78.

19) N.R.Tao, M. L. Sui, J. Lu, K. Lu, Surface Nanocrystallization of Iron Induced by Ultrasonic Shot Peening. Nanostructured Materials, Vol. 11, No. 4 (1999) 433-440.

20) R. Menig, L. Pintschovius, V. Schulze, Depth Profiles of Macro Residual Stresses in Thin Shot Peened Steel Plates Determined by X-ray and Neutron Diffraction. Scripta Materialia, 45 (2001) 977-983.

21) P.S. Song, C.C. Wen. Crack Closure and Crack Growth Behavior in Shot Peened Fatigue Specimen. Engineering Fracture Mechanics, 63 (1999) 295-304.

22) A. Drechsler, T. Dorr, L. Wagner, Mechanical Surface Treatments on Ti-10V-2Fe-3Al for Improved Fatigue Resistance. Materials Science and Engineering A, 243 (1998) 217-220.

23) N.R. Tao, Z.B. Wang, W.P. Tong, M.L. Sui, K. Lu, An Investigation of Surface Nanocrystallization Mechanism in Fe Induced by Surface Mechanical Attrition Treatment. Acta Materials, 50 (2002) 4603-4616.

24) L. Shaw, P.K. Liaw, A Novel Surface Nanocrystallization and Hardening (SNH) Process for Improved Fatigue and Wear Resistance. Proposal to the National Science Foundation.

25) H.W. Zhang, Z.K. Hei, G. Liu, J. Lu, K. Lu, Formation of Nanostructured Surface Layer on AISI 304 Stainless Steel by Means of Surface Mechanical Attrition Treatment. Acta Materialia, 51 (2003) 1871-1881.

26) K. Lu, J. Lu, Surface Nanocrystallization (SNC) of Metallic Materials-Presentation of the Concept Behind a New Approach. Journal of Materials Science & Technology, 15 (3) (1999) 193-197.

27) A. Vinogradov, S. Nagasaki, V. Patlan, K. Kitagawa, M. Kawazoe, Fatigue Properties of 5056 Al-Mg Alloy Produced by Equal-Channel Angular Pressing. Nanostructured Materials, Vol. 11, No.7 (1999) 925-934.

28) T. Hanlon, Y.-N. Kwon, S. Suresh, Grain Size Effects on the Fatigue Response of Nanocrystalline Metals. Scripta Materiallia, 49 (2003) 675-680.

29) ASTM C 1211-98a: Standard Test Method for Flexural Strength of Advanced Ceramics at Elevated Temperatures. ASTM Standards, 1998.

30) G.F.V. Voort, Metallography: Principles and Practice, Materials Science and Engineering Series, ed., Bever, M.B., 1984, New York: McGraw-Hill Book Company.

31) J.H. He, E.J. Lavernia, Development of Nanocrystalline Structure during Crymilling of Inconel 625. J. Mater. Res., 16 (9) (2001) 2724-2732.

32) C. Suryannarayana, E. Ivanov, V.V. Boldyrev, The Science and Technology of Mechanical Alloy. Materials Science and Engineering A, 304-306 (2001) 151-158.

33) L. Shaw, H. Luo, J. Villegas, D. Miracle, Thermal Stability of Nanostructured Al93Fe3Cr2Ti2 Alloys Prepared via Mechanical Alloy. Acta Materiallia, 2003, in press.

34) J. Villegas, K. Dai, L. Shaw, Surface Roughness Evolution in the Surface Nanocrystallization and Hardening (SNH) Process, in *Processing and Fabrication of Advanced Materials: XII,* T.Srivatsan and R.Varin, Eds., ASM International, Materials Park, OH, October 2003 (in press).

Appendices

Appendix A

Tables

Table 1 Chemical Composition of the Ti-6Al-4V Alloy

Element	Ti	Al	V	O	Fe	N	Other
Weight Percent	Balance	5.5 - 6.8	3.5 - 4.5	0.10 max.	0.4 max.	0.05 max.	0.4 max.

Table 2 Chemical Composition of the Ni-Based Hastelloy® C-2000 Superalloy

Element	Ni	Cr	Mo	Co	C	Si
Weight Percent	Balance	23	16	1.6	0.01 max.	0.08 max.

Table 3 Mechanical Properties of the Ti-6Al-4V and Ni-Based Hastelloy® C-2000 Alloys

	Yield strength (MPa)	Tensile strength (MPa)	Young's modulus (MPa)
Ti-6Al-4V	934	993	117,000
Hastelloy® C-2000	393	765	198,600

Table 4 Parameters Used by the SMA Treatment

Materials of Balls	The number of the Balls	Diameter of Balls (mm)	Processing Time (min.)	Processing Atmosphere	Processing Temperature (º C)
Steel or WC	5	7.9 or 4.88	30, 60, or 180	Ar	24

Table 5 Chemical Composition of 440C Steel Balls

Element	Cr	C	Si	Mo	Mg	P	S	Fe
Weight Percent	16 - 18	0.95 - 1.20	1.00 max.	0.75 max.	0.10 max.	0.04 max.	0.03 max.	Balance

Table 6 Parameters of the SMA Process for the Ni-Based Hastelloy® C-2000 Superalloy

	Ball Material	Ball number	Diameter (mm)	Treated time (min.)	Atmosphere
Lot 1	WC	5	7.9	30	Ar
Lot 2	WC	5	7.9	180	Ar
Lot 3	WC	5	4.88	60	Ar

Table 7 Dimensions of the Disks for the SMA Treatment

	Diameters of Whole Disk (mm)	Thickness of the Disk (mm)	Diameters of the Treated Area (mm)
Ti-6Al-4V	49	5.0	30
Hastelloy® C-2000	49	3.22	30

Table 8 Dimensions of the Fatigue Specimen

	Length (mm)	Depth (mm)	Width (mm)
Ti-6Al-4V	25	2.5	2.0
Hastelloy® C-2000	25	3.22	3.22

Appendix B

Figures

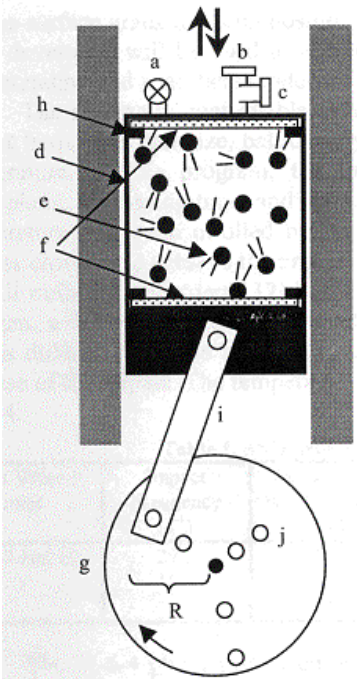

Figure 1 Schematic of a machine for the SMA process, d is the process chamber; g, a rotating disk connected to an electric motor; f, metallic plates to be processed; and e, flying balls [24]

Figure 2 Spex mill 8,000 for the SMA treatment

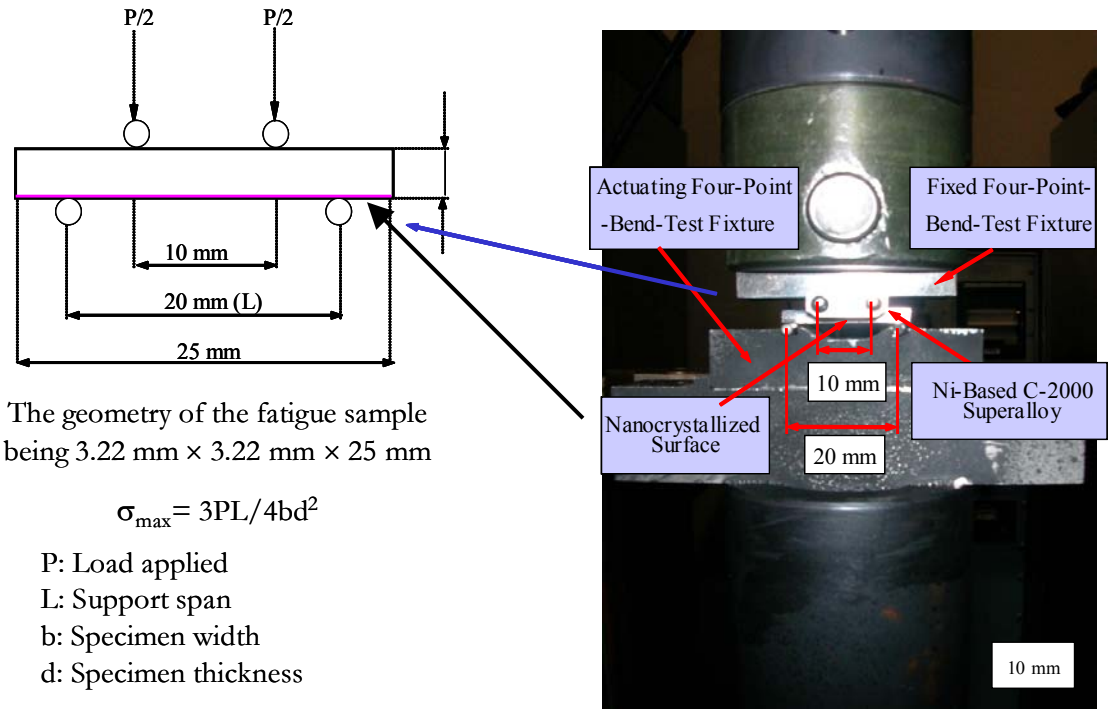

The geometry of the fatigue sample being 3.22 mm × 3.22 mm × 25 mm

$$\sigma_{max} = 3PL/4bd^2$$

P: Load applied
L: Support span
b: Specimen width
d: Specimen thickness

Figure 3 Fixtures for the four-point-bend-fatigue test

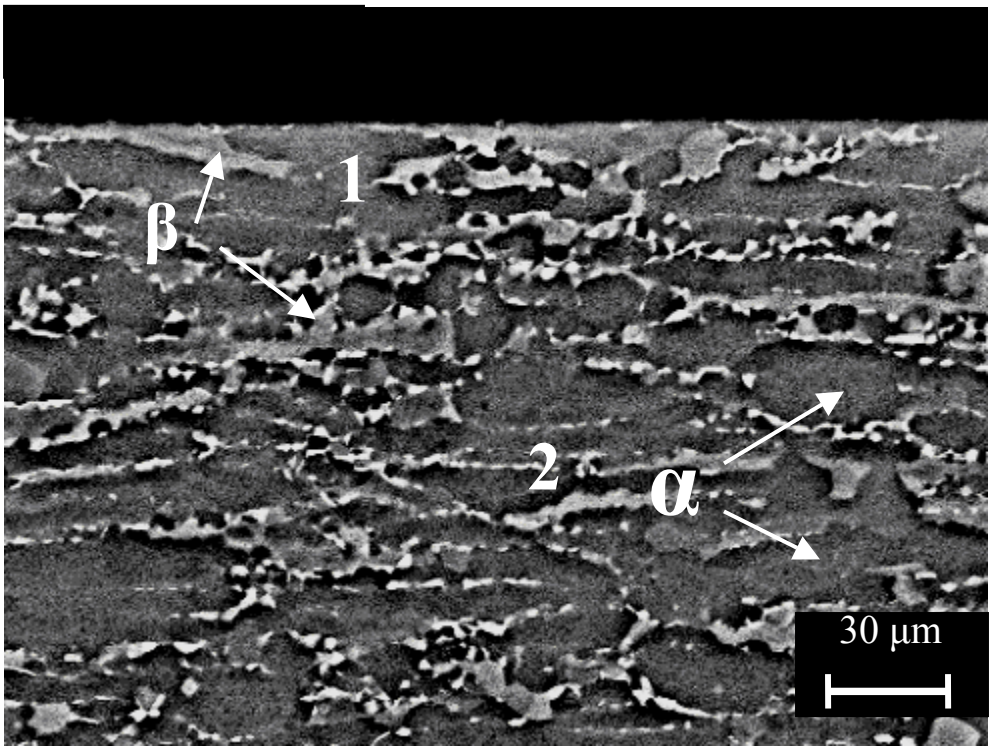

Figure 4 Microstructure of the cross section of the as-received Ti-6Al-4V alloy, the raised part is beta phase, and the depressed part is the alpha phase, 1 is the near-surface zone, and 2 is in the interior

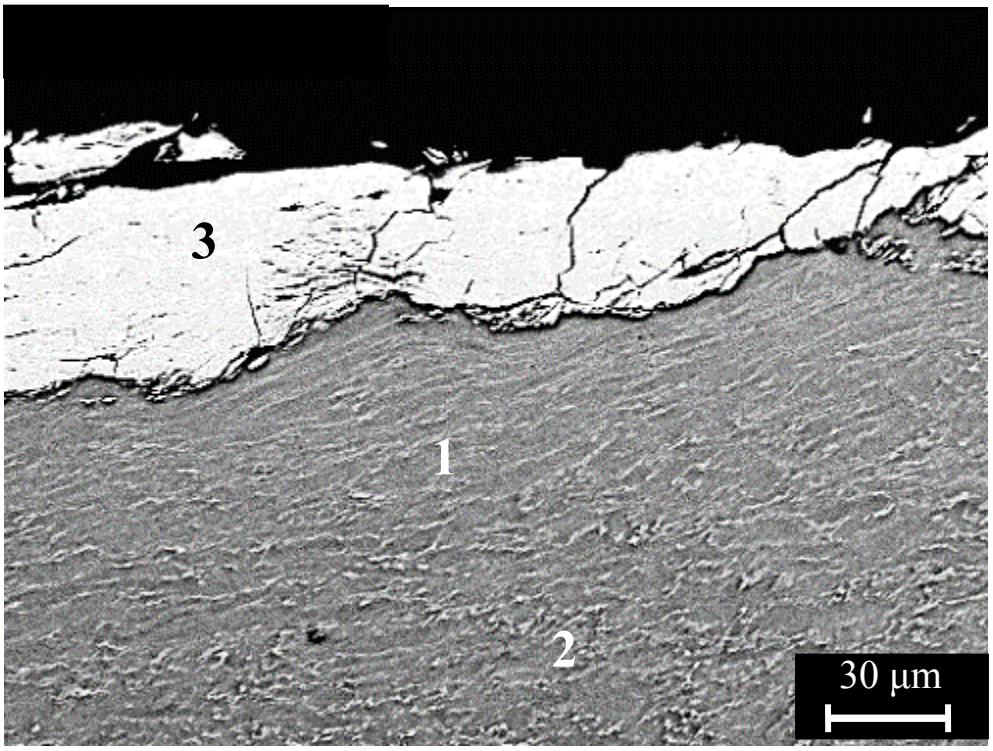

Figure 5 Microstructure of the cross section of the treated Ti-6Al-4V alloy, 1 is the near-surface zone (SMA affected zone), 2 is in the interior (SMA-unaffected zone), and 3 is the white layer (adhesion-fracture region)

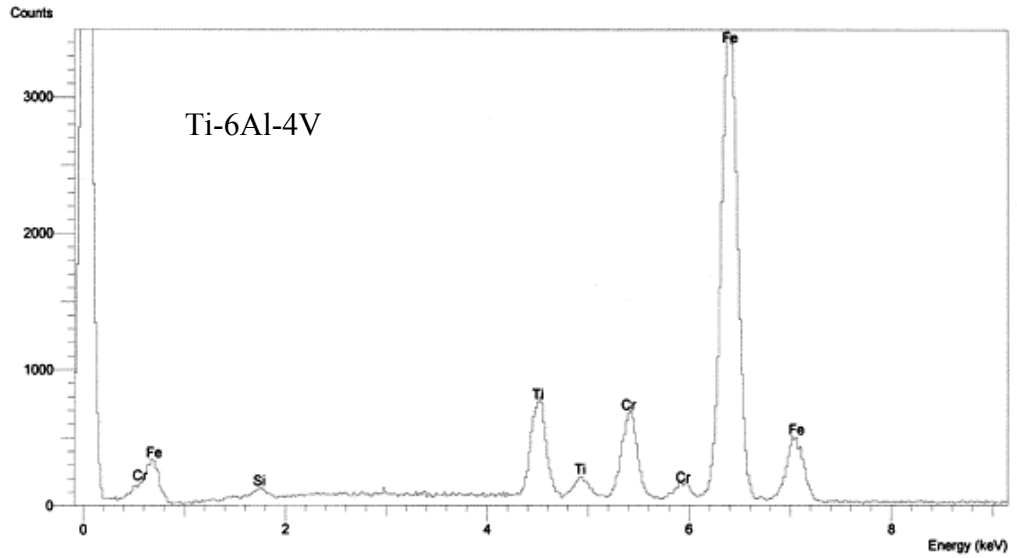

(a) EDS of the white layer

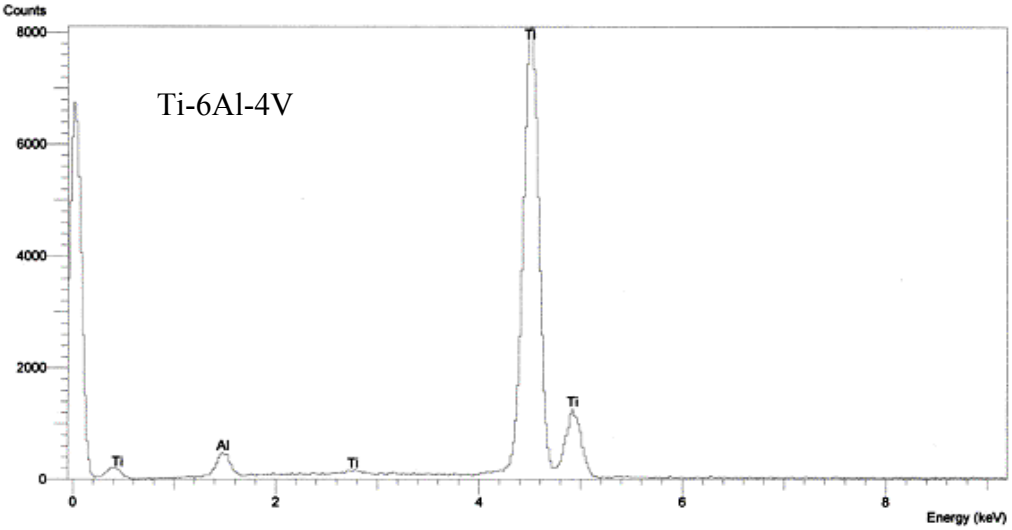

(b) EDS of the alpha phase (depressed phase)

Figure 6 EDS of (a) the white layer, (b) the alpha phase, and (c) the beta phase in Figure 5

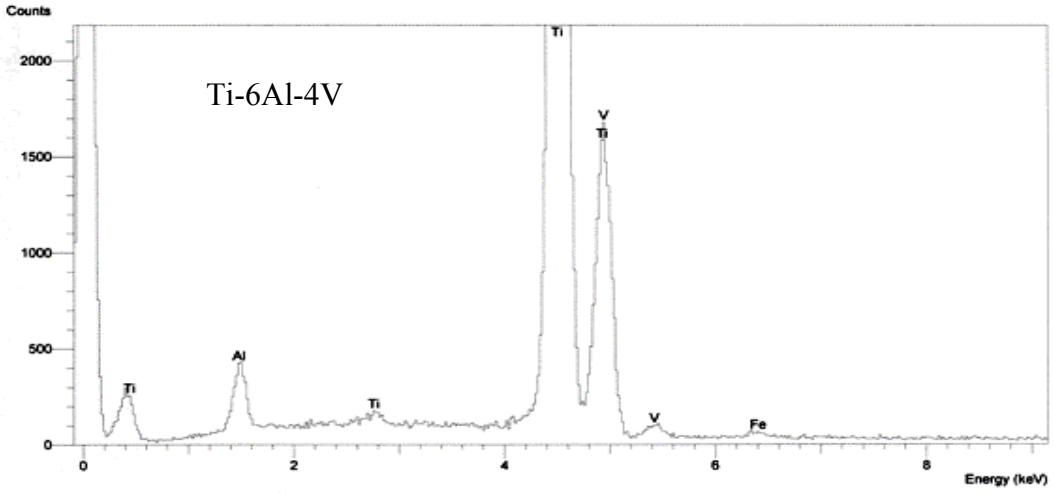

(c) EDS of the beta phase (raised phase)

Figure 6 Continued

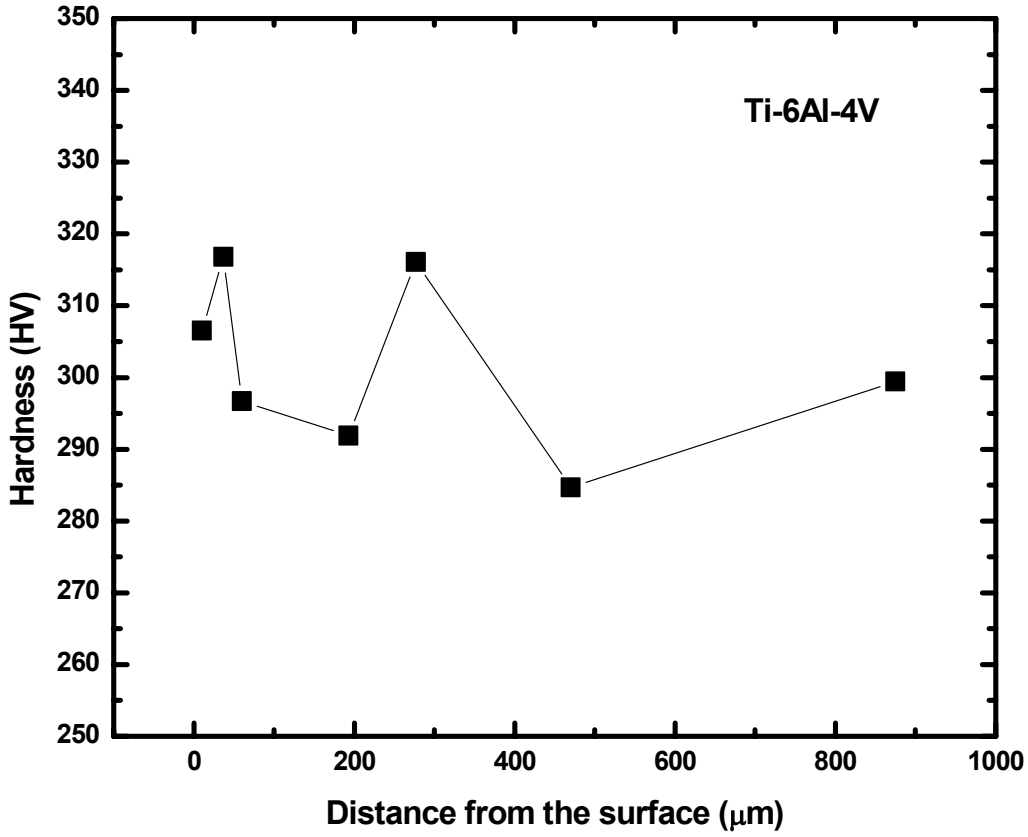

Figure 7 Microhardness profile of the treated Ti-6Al-4V sample along the cross section

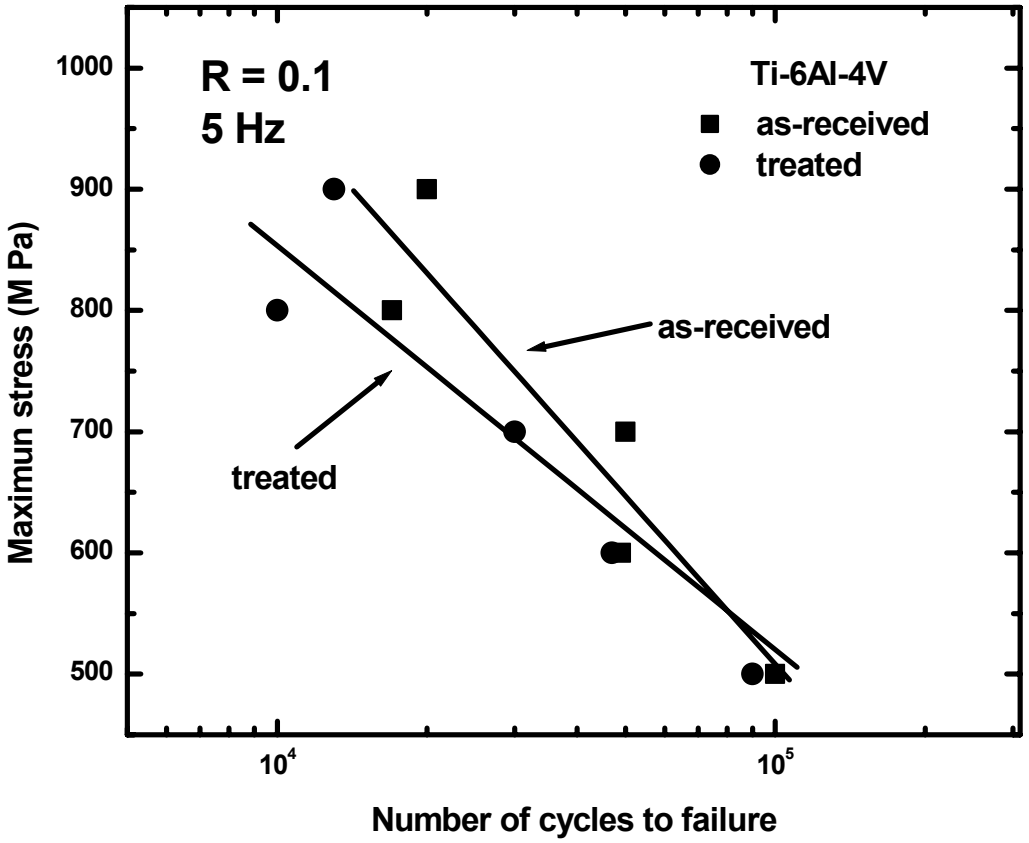

Figure 8 Fatigue results of the as-received and as-treated samples of the Ti-6Al-4V alloy

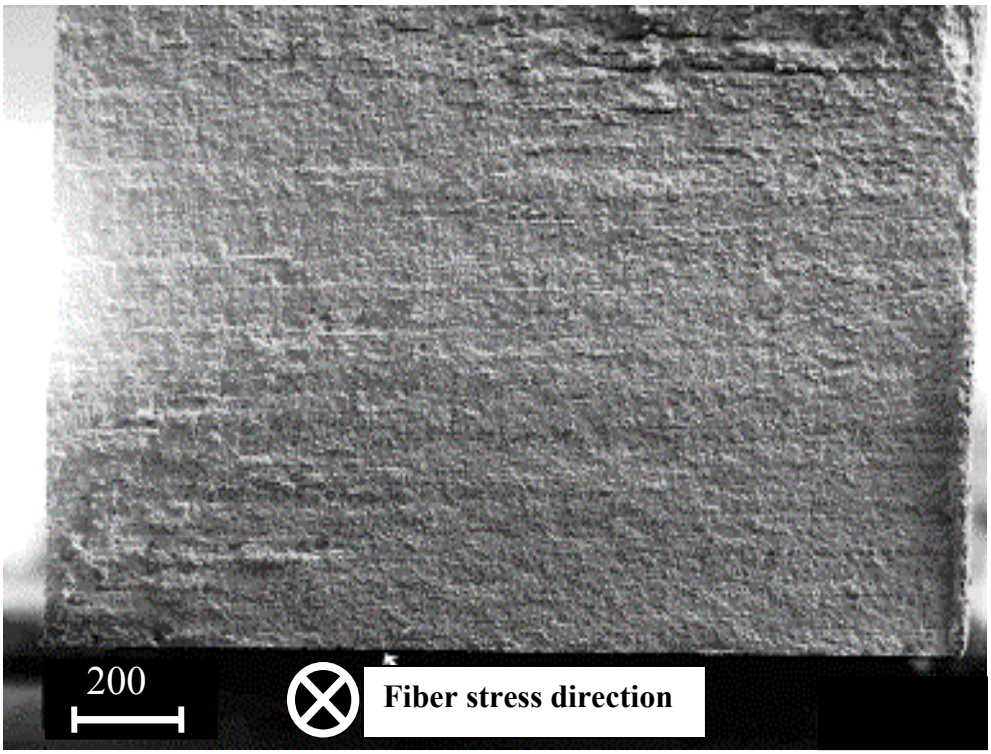

Figure 9 Fatigue-fracture surface of the as-received Ti-6Al-4V alloy (SEM), the fiber stress direction is perpendicular to the fracture surface

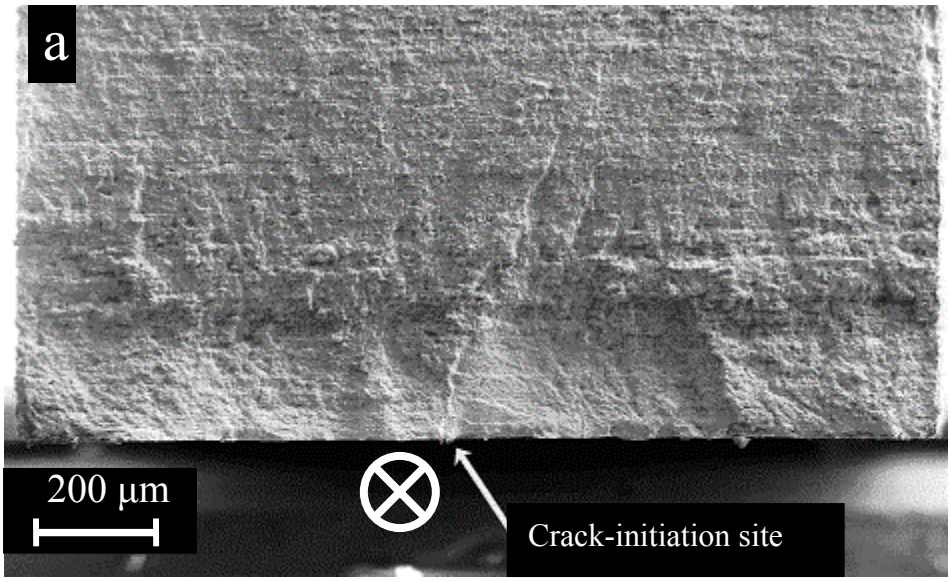

(a) Fatigue-fracture surface of the treated Ti-6Al-4V alloy

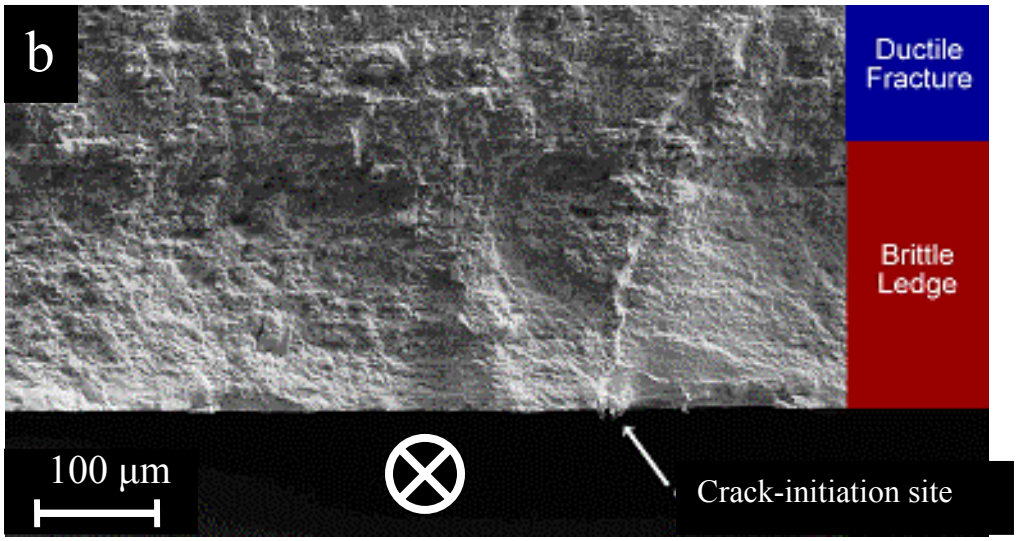

(b) Fatigue-fracture surface of the treated Ti-6Al-4V alloy with a higher magnification

Figure 10 Fatigue-fracture surfaces of the treated Ti-6Al-4V alloy, the fiber stress direction is perpendicular to the fracture surface

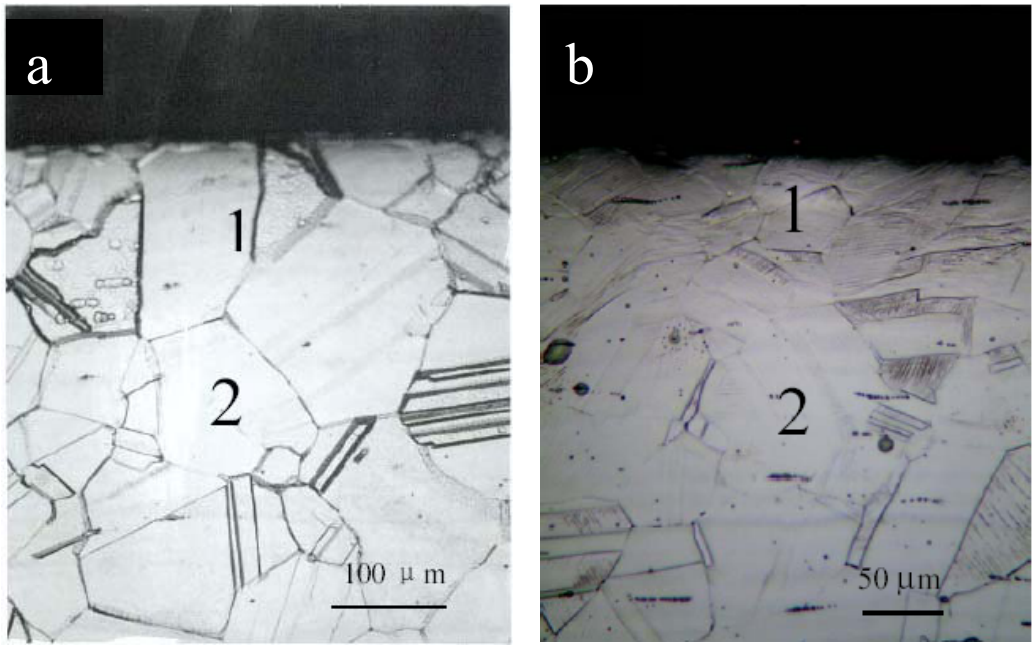

Figure 11 Optical images of the cross-sectional microstructures of Ni-based Hastelloy® C-2000 samples, (a) as-received, (b) treated 30 min. with 7.9 mm balls, (c) treated 180 min. with 7.9 mm balls, and (d) treated 60 min. with 4.88 mm balls, 1 is the near-surface zone, and 2 is in the interior

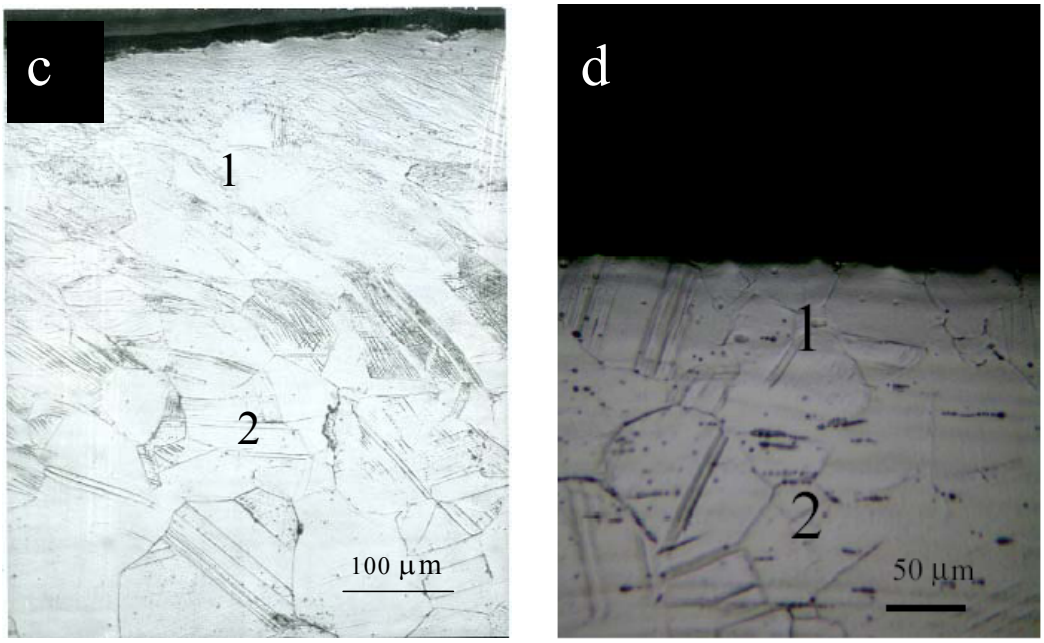

Figure 11 Continued

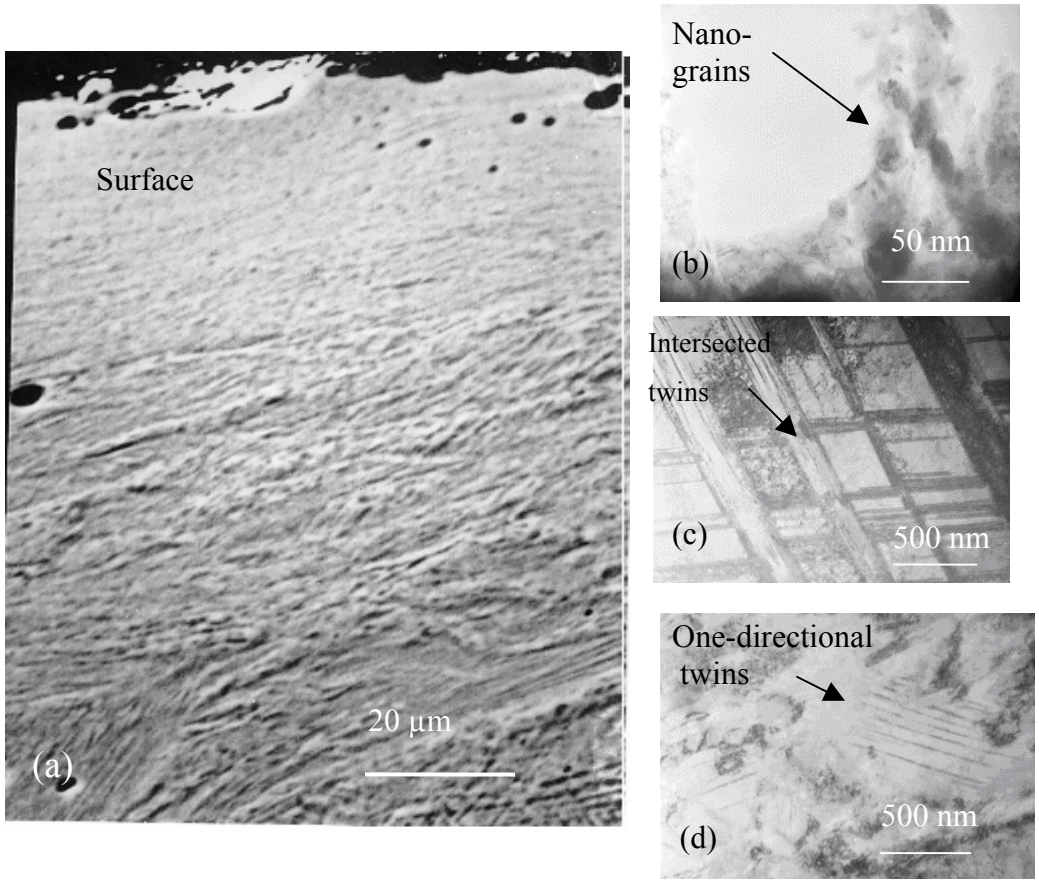

Figure 12 Detailed surface structures of the treated 180 min. Ni-based Hastelloy® C-2000 sample, (a) SEM image of the SNH-affected zone, (b) nano-grains, (c) intersected plastically-deformed twins, and (d) one-directional plastically-deformed twins

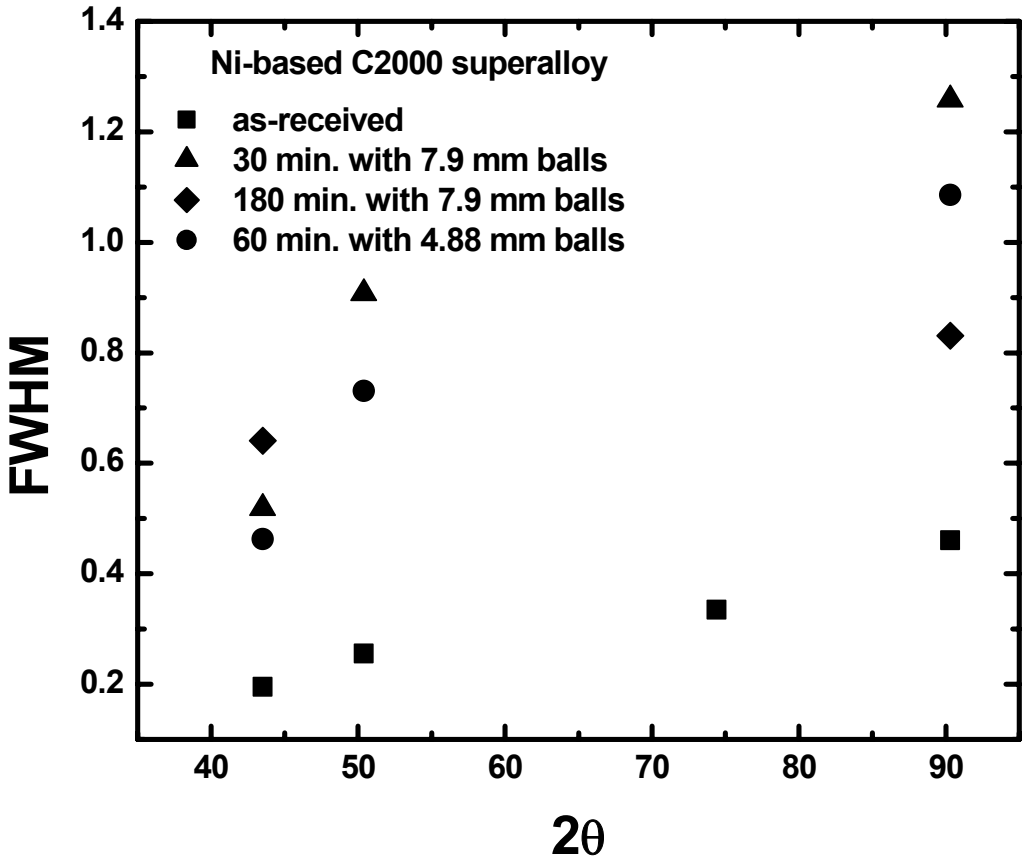

Figure 13 Full width at half maximum (FWHM) changes of the X-ray peaks of the four Ni-based Hastelloy® C-2000 sample surfaces

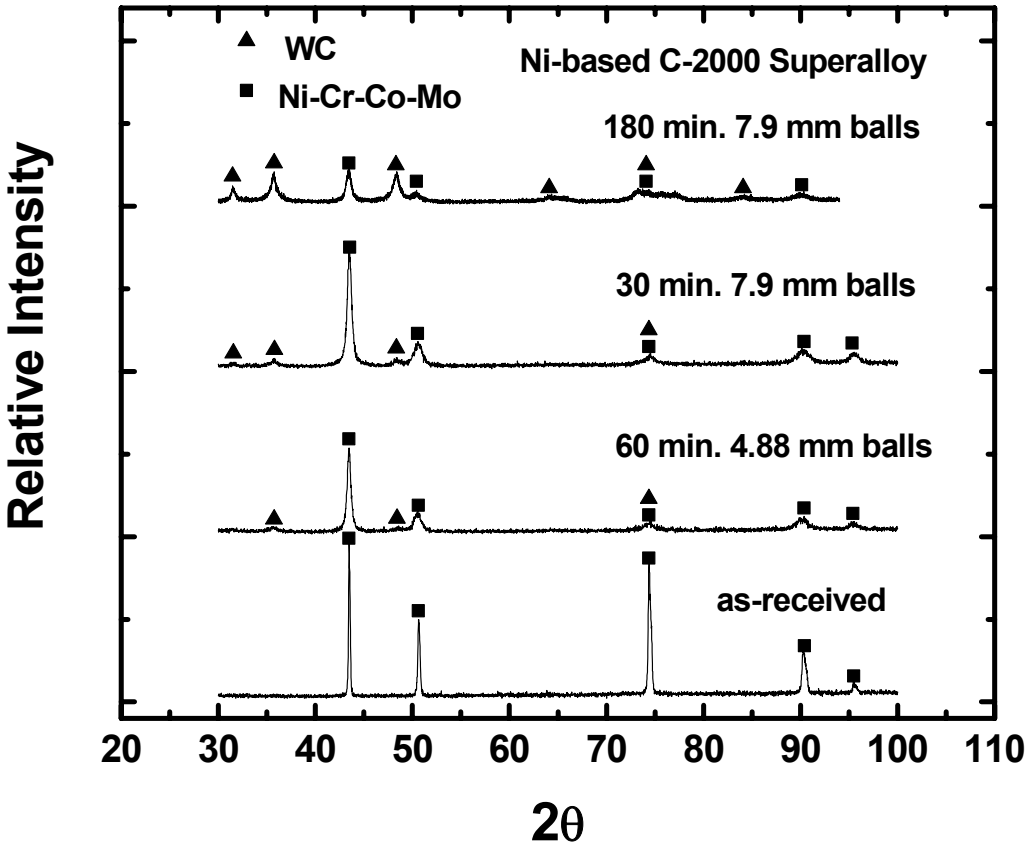

Figure 14 XRD profiles of the as-received and SMA-treated Ni-based Hastelloy® C-2000 samples

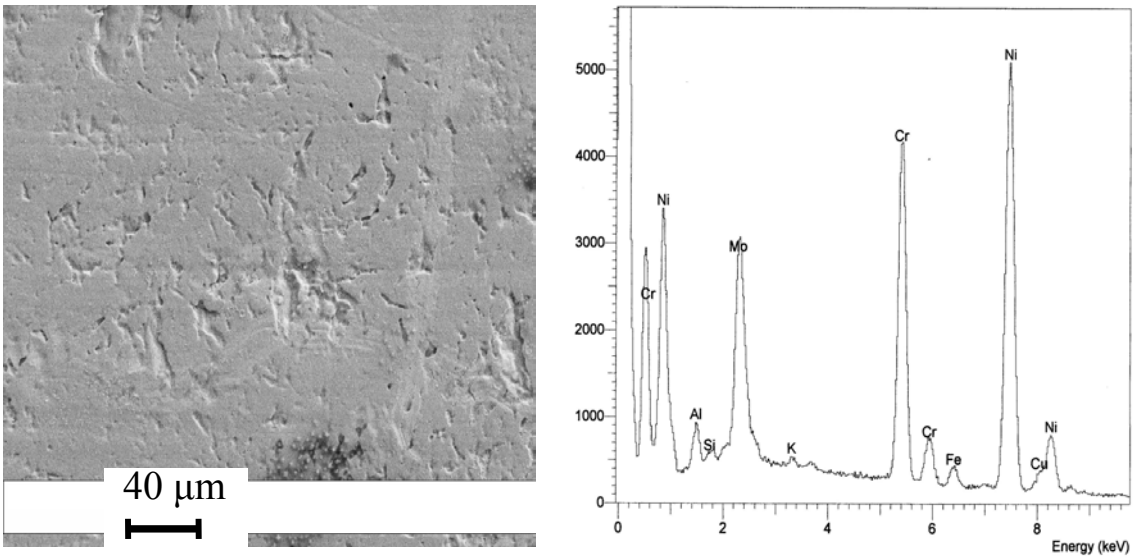

(a) As-received sample

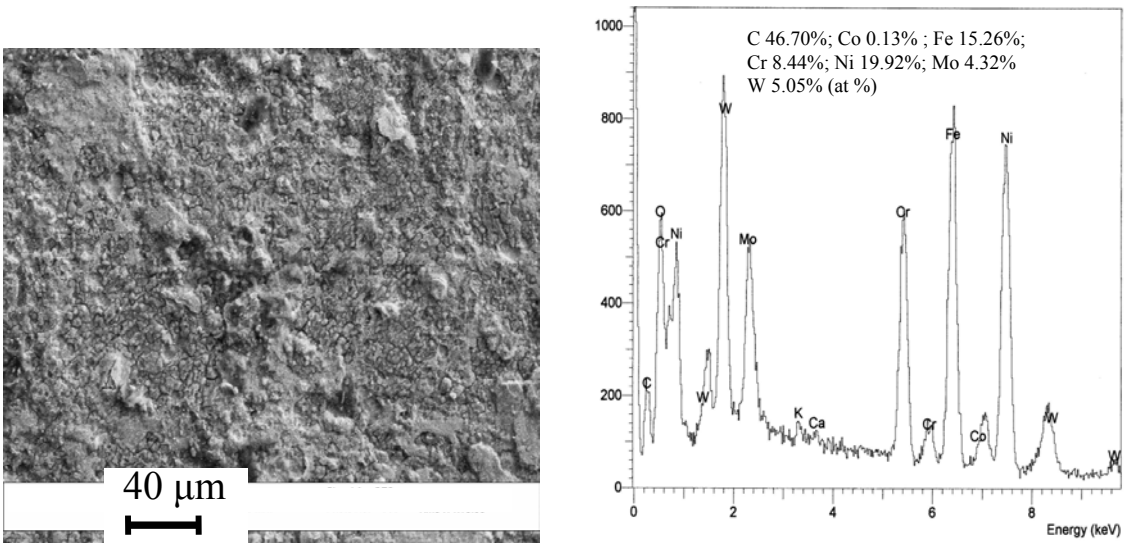

(b) Treated 30 min. sample with five WC balls in a 7.9 mm diameter

Figure 15 Surface appearances and EDS spectra of Ni-based Hastelloy® C-2000 samples, (a) as-received sample, (b) treated sample 30 min. with 7.9 mm balls, (c) treated 180 min. sample with 7.9 mm balls, and (d) treated 60 min. sample with 4.88 mm balls

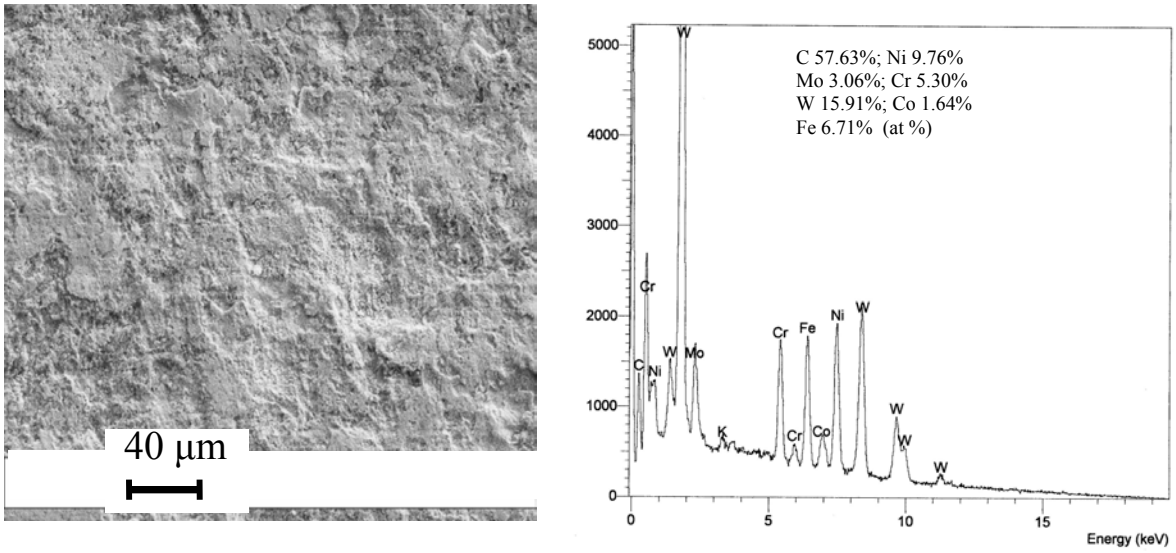

(c) Treated 180 min. sample with 5 WC balls in a 7.9 mm diameter

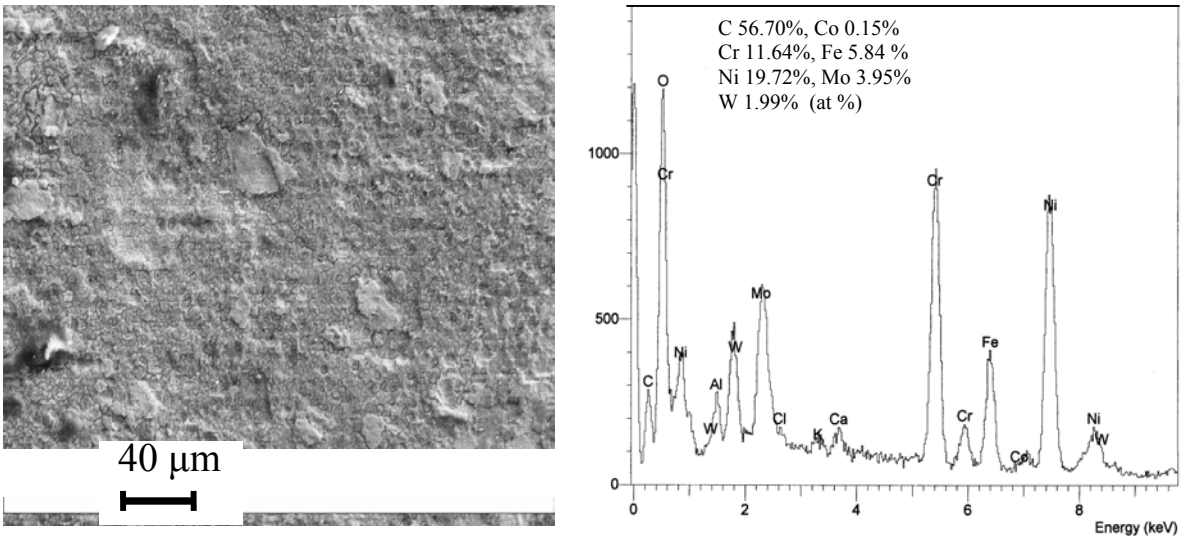

(d) Treated 60 min. sample with 5 WC balls in a 4.88 mm diameter

Figure 15 Continued

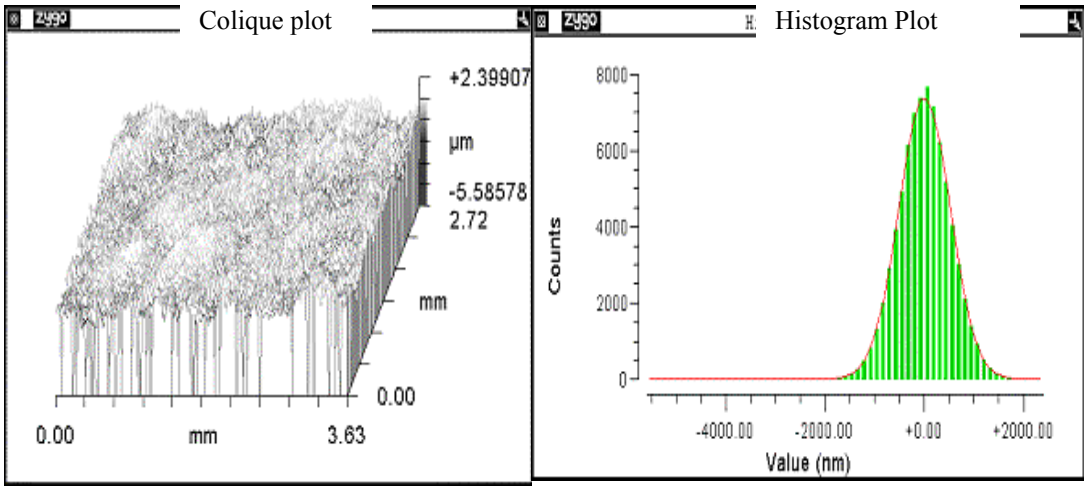

As-received sample

(PV = 7.985 µm; rms = 0.519 µm; Ra = 0.411 µm)

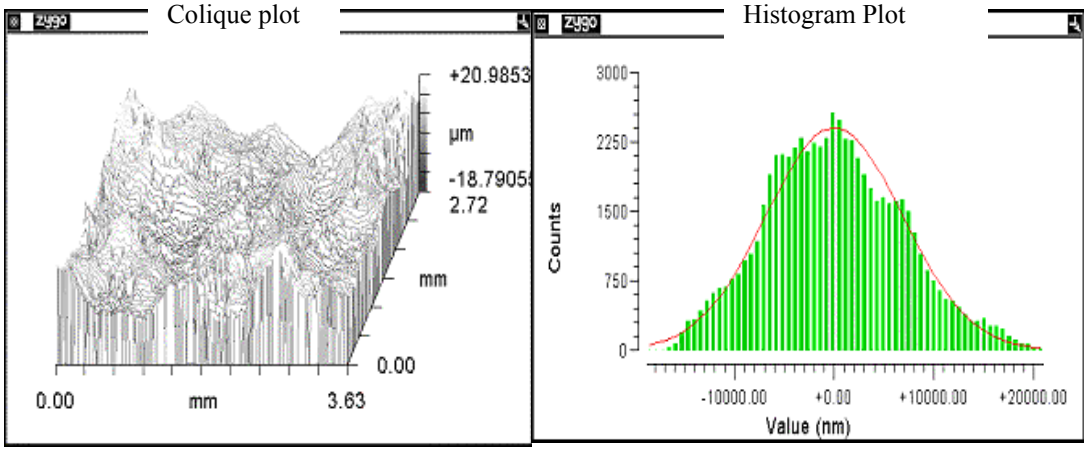

Treated 30 min. sample with 5 WC balls in a diameter of 7.9 mm

(PV = 39.776 µm; rms = 6.835 µm; Ra = 5.504 µm)

Figure 16 Surface roughnesses of the as-received and treated Ni-based Hastelloy® C-2000 samples

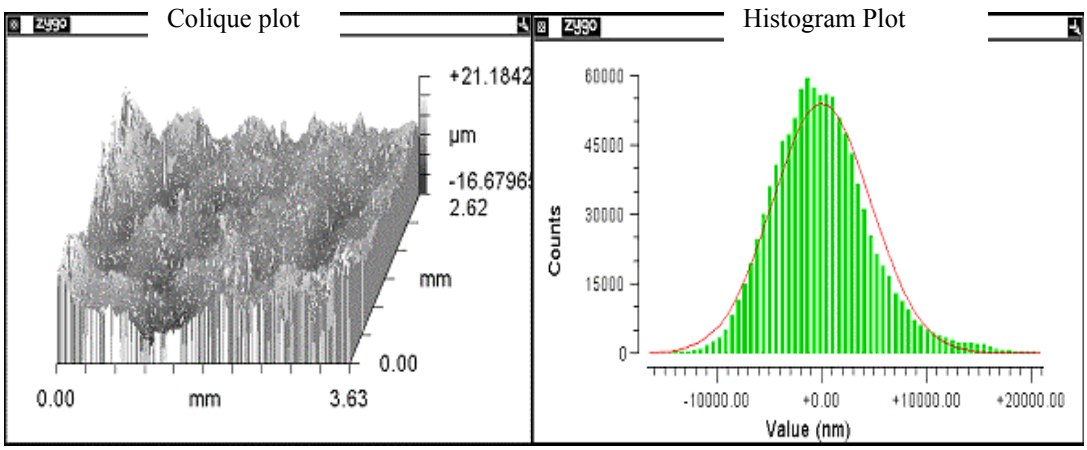

Treated 180 min. sample with 5 WC balls in a diameter of 7.9 mm

(PV = 37.864 µm; rms = 4.688 µm; Ra = 3.636 µm)

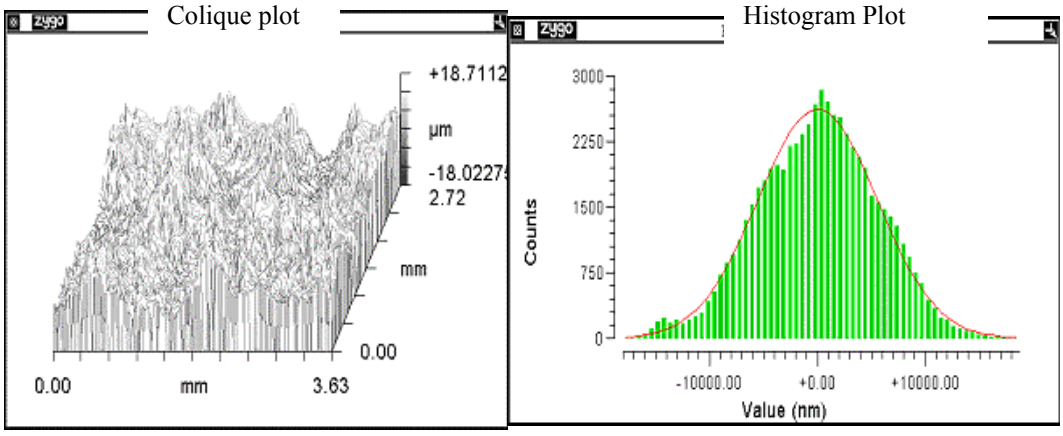

Treated 60 min. sample with 5 WC balls in a diameter of 4.88 mm

(PV = 36.734 µm; rms = 5.512 µm; Ra = 4.420 µm)

Figure 16 Continued

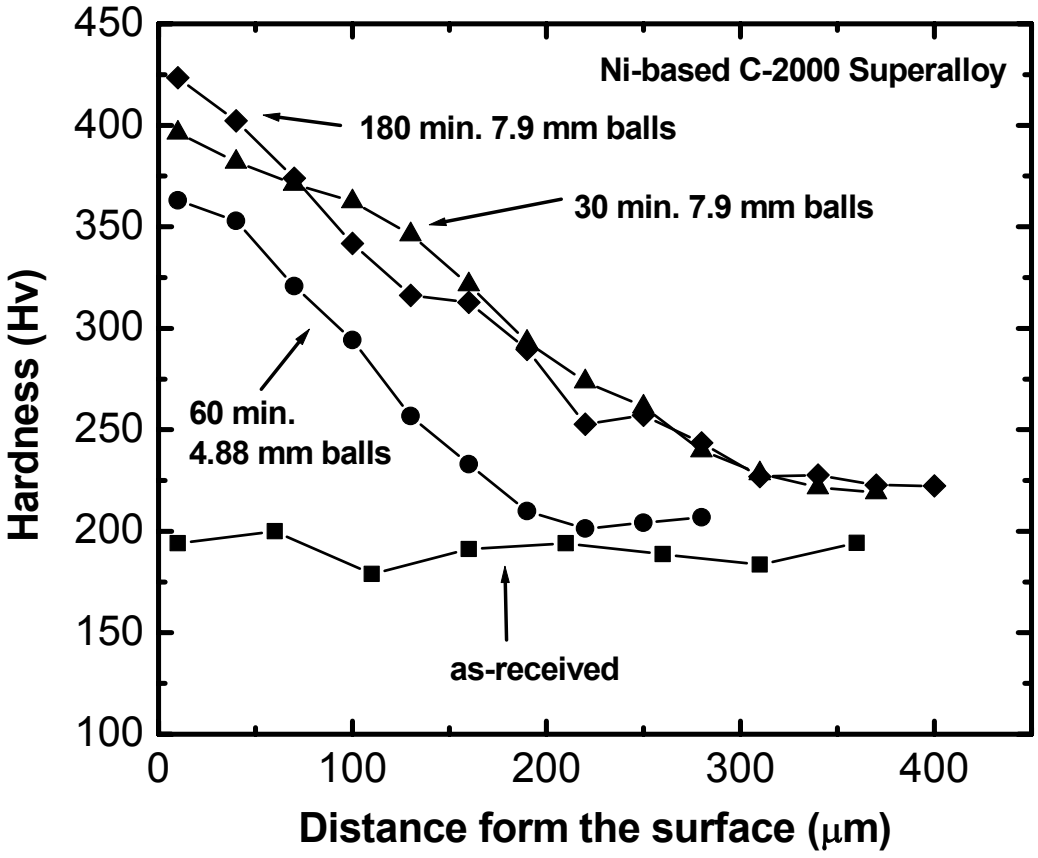

Figure 17 Microhardness profiles along the cross sections of the four Ni-based Hastelloy® C-2000 samples

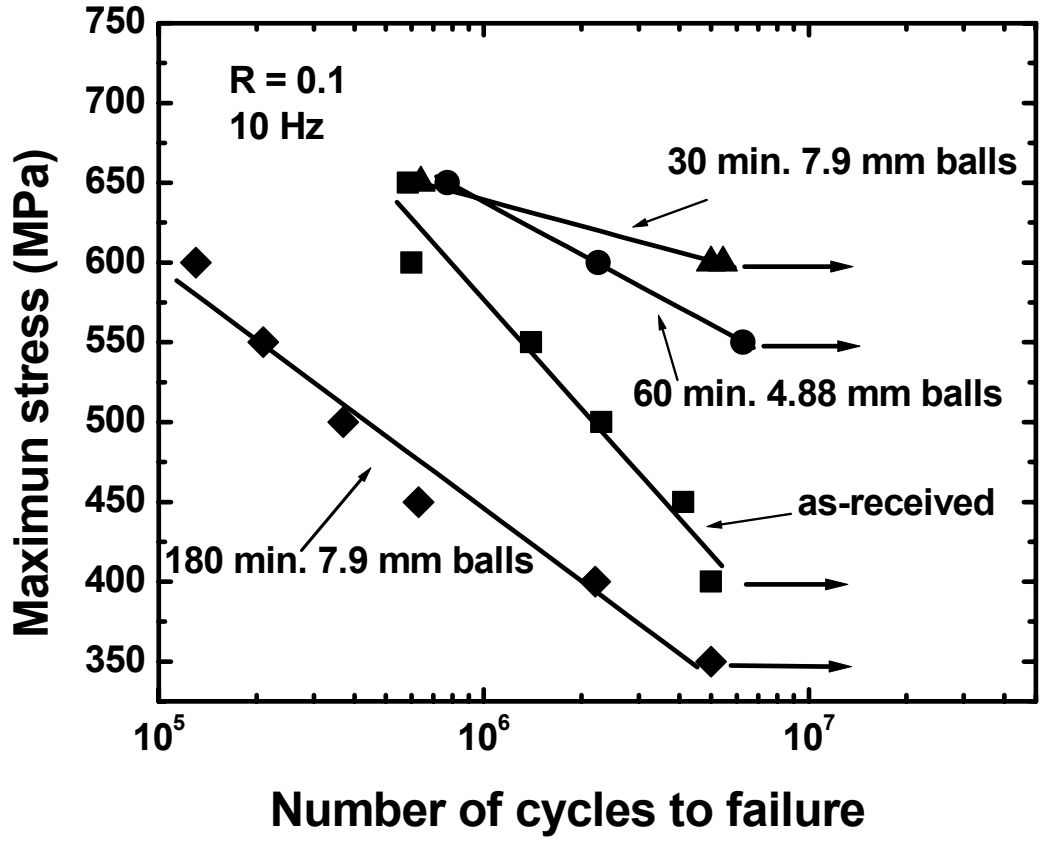

Figure 18 Fatigue results of the four Ni-based Hastelloy® C-2000 samples

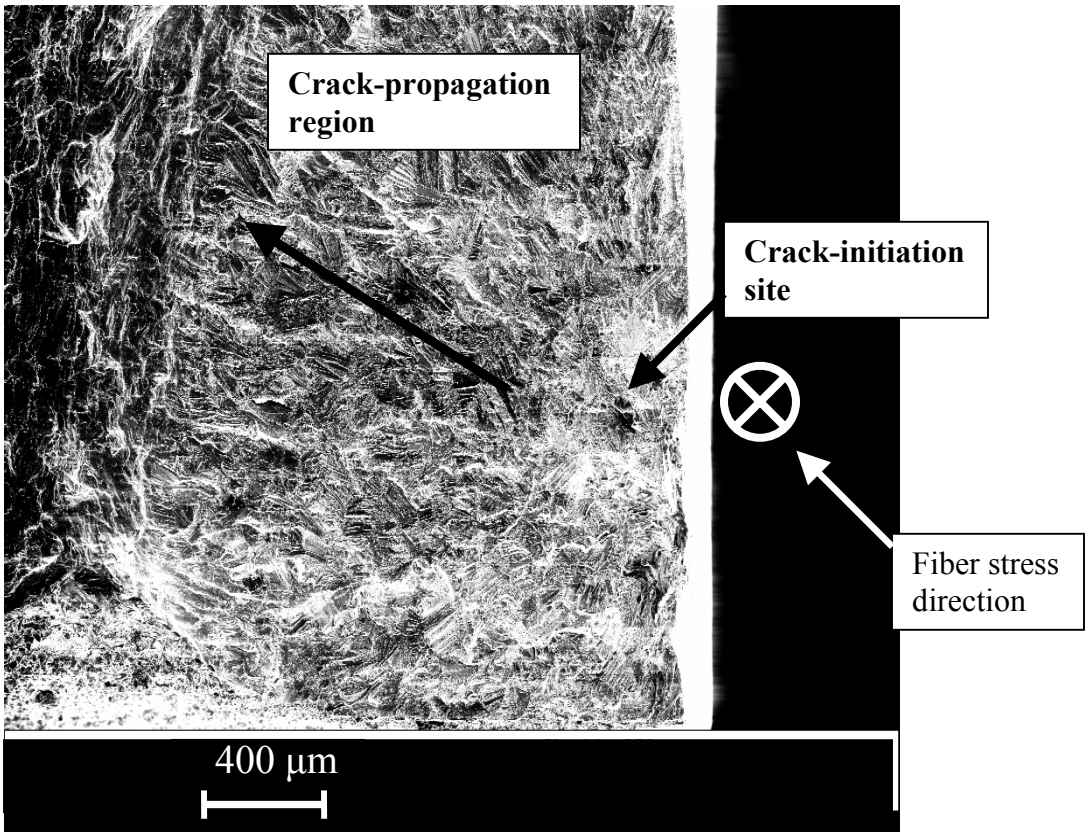

(a) Fracture surface with a crack-initiation site and fatigue-crack-propagation region.

Figure 19 Fatigue-fracture surface of the as-received Ni-based Hastelloy® C-2000 sample, the fiber stress direction is perpendicular to the fracture surface

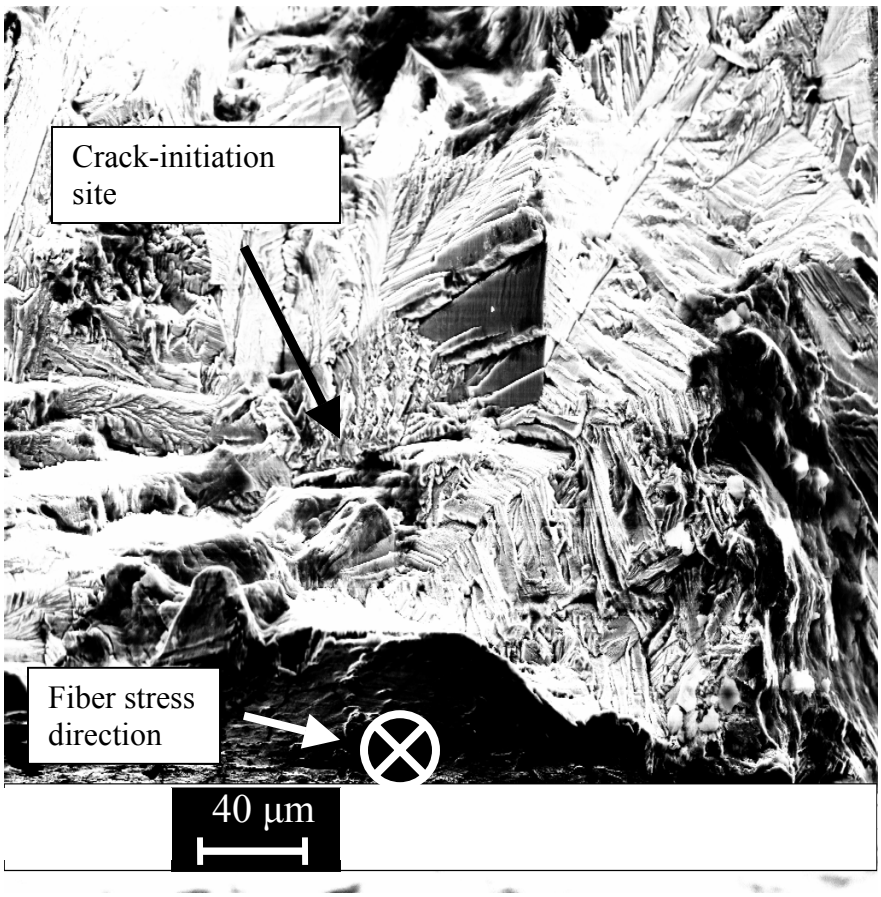

(b) Image of the fatigue-crack-initiation site

Figure 19 Continued

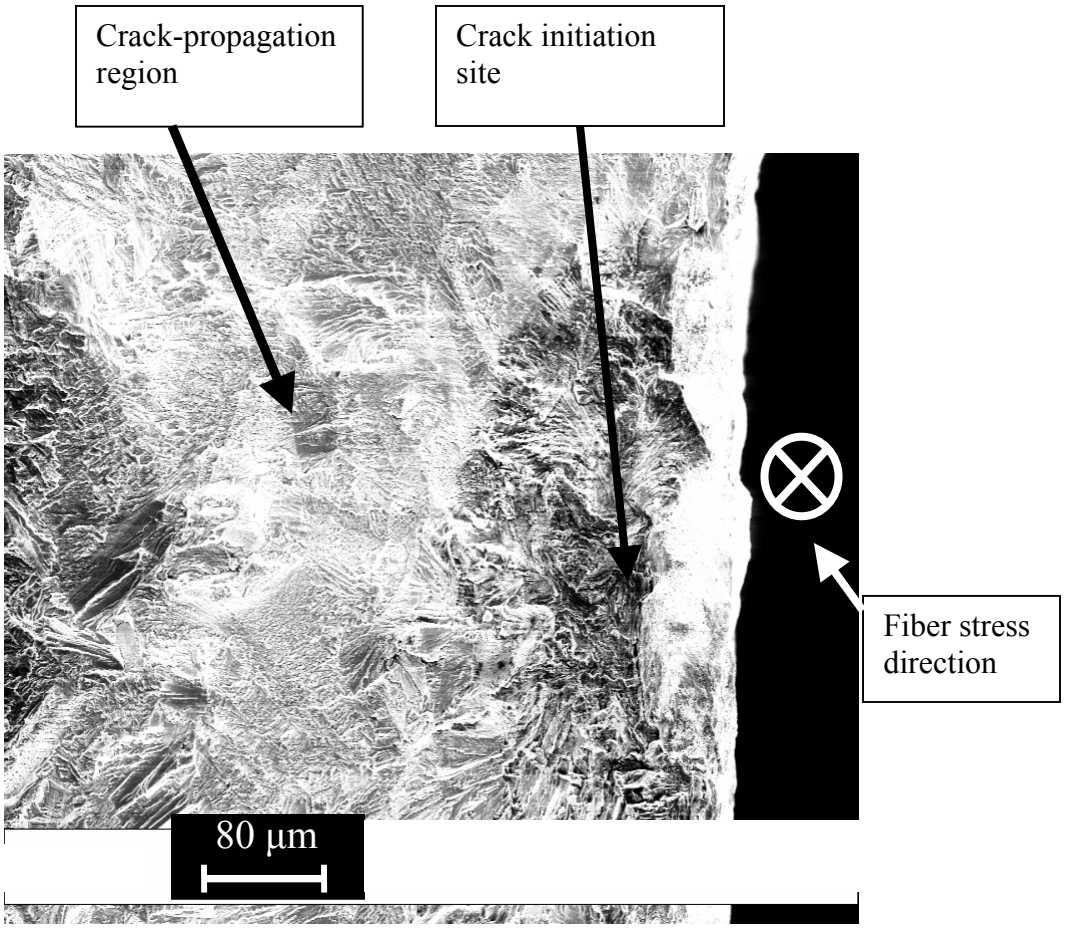

Figure 20 Fatigue-fracture surface of treated 30 min. Ni-based Hastelloy® C-2000 sample with 5 WC balls in a 7.9 mm diameter, the fiber stress direction is perpendicular to the fracture surface

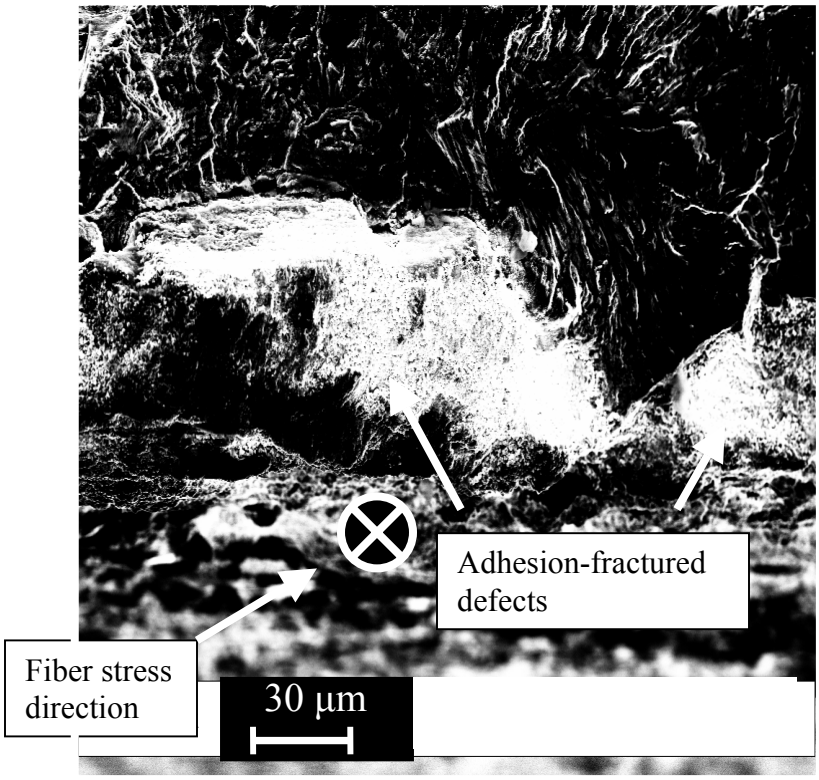

(a) Crack-initiation site

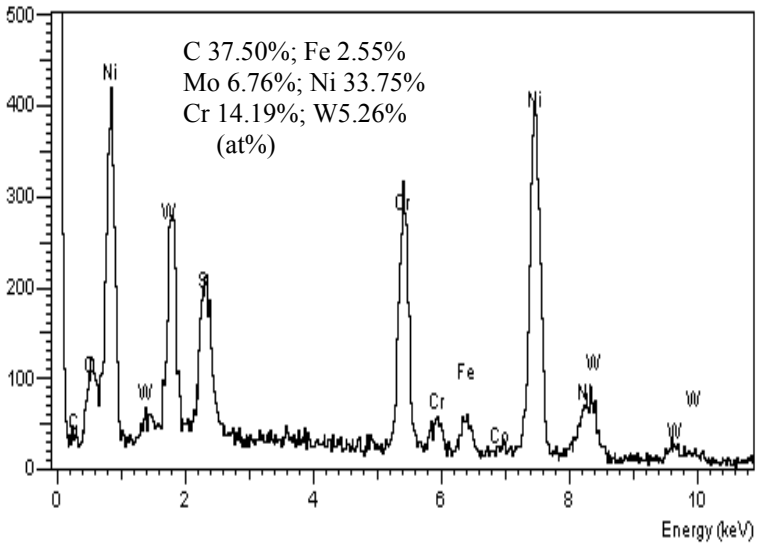

(b) EDS of the adhesion-fractured defects

Figure 21 Crack initiation site (a) and EDS of the adhesion-fractured defects (b) of the treated 30 min. sample with 7.9 mm balls

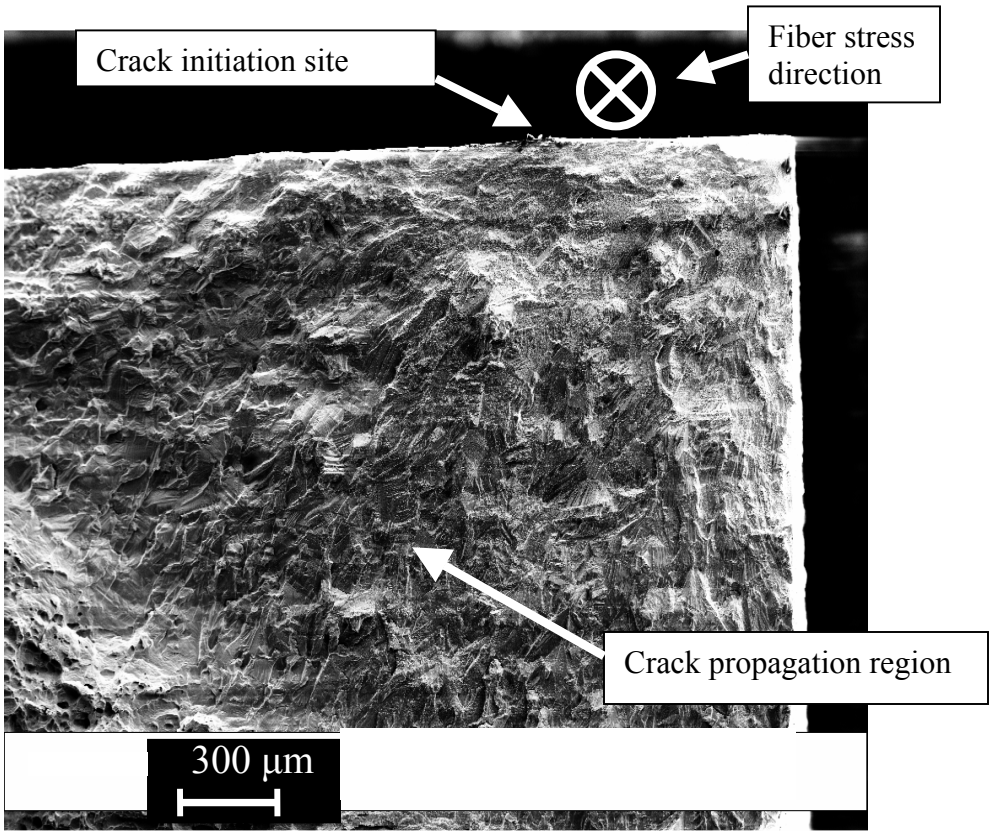

Figure 22 Fracture surface of the treated 180 min. sample with 7.9 mm balls, the fiber stress direction is perpendicular to the fracture surface

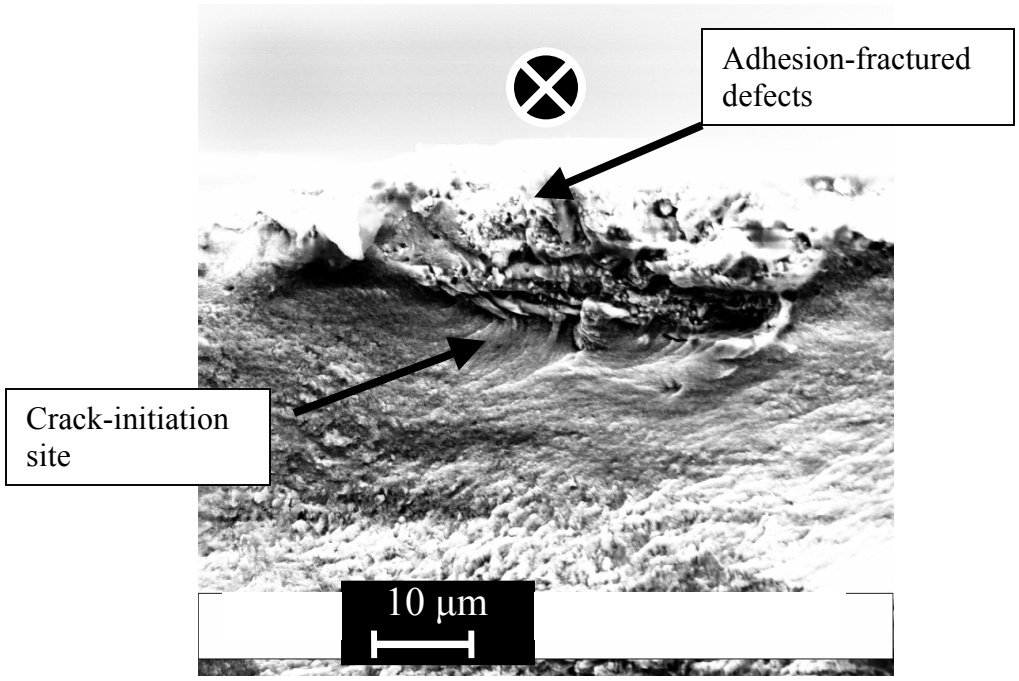

(a) Crack-initiation site

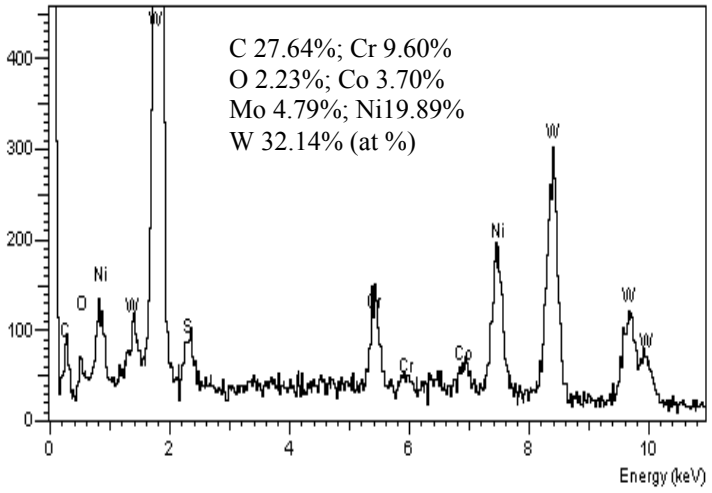

(b) EDS of the adhesion-fractured defects

Figure 23 Crack-initiation site (a) and EDS of the adhesion-fractured defects (b) of the treated 180 min. sample with 7.9 mm balls, the fiber stress direction is perpendicular to the fracture surface

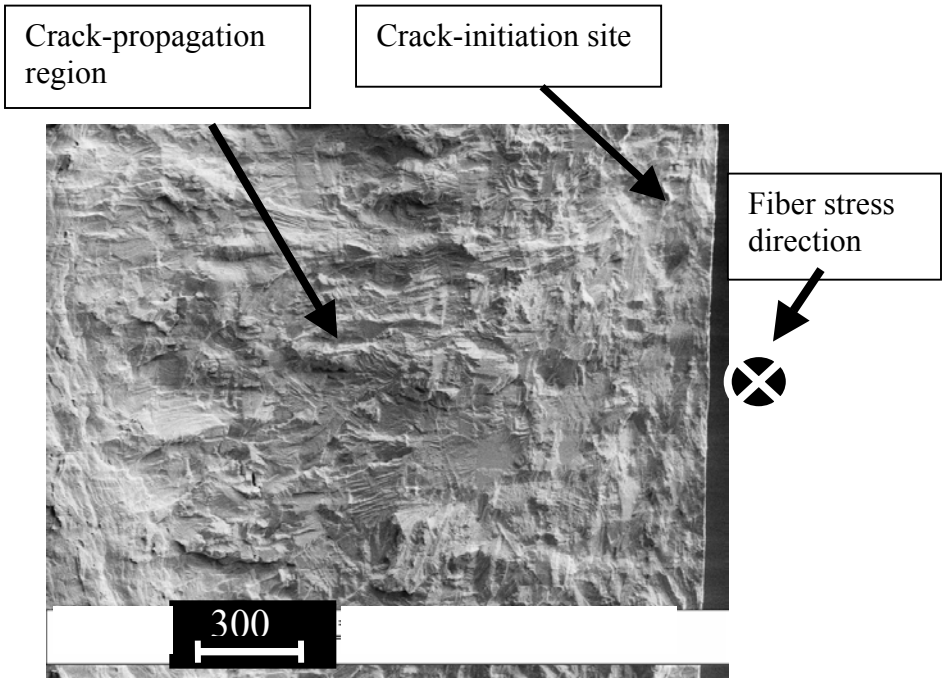

(a) Fracture surface with fatigue-crack-propagation region

Figure 24 Fatigue-fracture surface of treated 60 min. Ni-based Hastelloy® C-2000 sample with 5 WC balls in 4.88 mm diameter, the fiber stress direction is perpendicular to the fracture surface

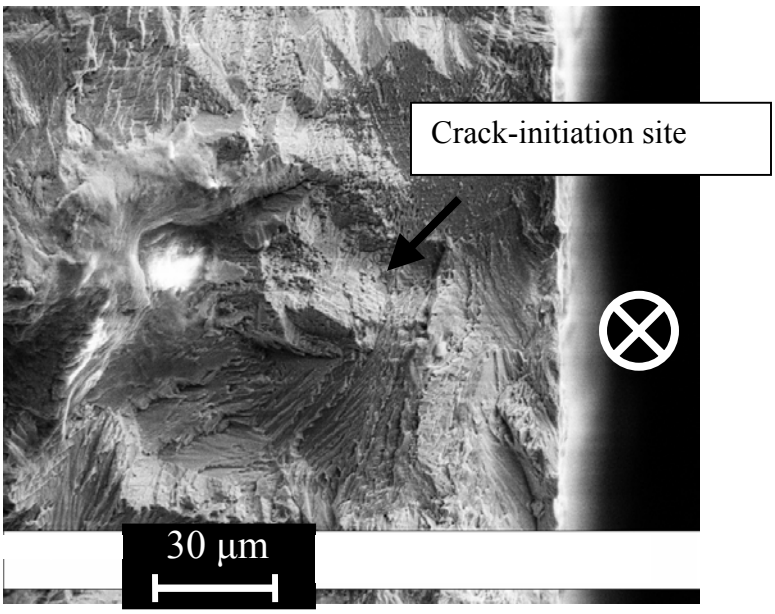

(b) Image of the fatigue-crack-initiation site

Figure 24 Continued

Vita

Wei Yuan was born in Zaozhuang, Shandong Province, People's Republic of China (PRC). During September 1994 to August 2002, he was pursuing his undergraduate study and master graduate study at Tsinghua University, Beijing, PRC, where he received his Bachelor of Science and Master of Science degrees in Materials Science and Engineering program.

He came to the University of Tennessee and enrolled in the Master Program in Materials Science and Engineering Department in 2002. The master degree will be received in August 2004.